NAPL DISSOLUTION[1]

1.   INTRODUCTION

Already at the beginning of contaminated site investigation and remediation it became obvious how challenging it is to decontaminate a polluted site within a "short" time frame (< decades). At many contaminated sites, remediation could be achieved within a decade (Travis and Doty, 1990; Travis and Macinnis, 1992). Meanwhile it is clear that remediation often takes many decades (if not centuries). Besides slow diffusion over large distances, slow dissolution kinetics of NAPLs are responsible for the persistence of subsurface contaminations. The dissolution rate of NAPL depends on their surface to volume ratio (blobs or ganglia or pools) and is limited by mass transfer across the NAPL/water interface. Large coherent volumes of NAPL (oil layers, DNAPL pools) take long times to dissolve as summarized for different scenarios in Table 1.

Tab. 1: Time scales for contaminant removal with remediation options (from Eberhard and Grathwohl, 2002, Grathwohl, 1998, Groundwater Quality Conference)

Scenario	Chlorinated solvents; BTEX	PAHs
Dissolved and sorbed contaminants		
Time scale for diffusion limited de-sorption at the grain scale	**< 1 years**	**1 – > 10 years**
Time scale for slow diffusion out of low permeability zones – matrix diffusion	**> 10 years**	**> 100 years**
Change of release rates / contaminant concentrations with time	Diffusive fluxes and concentrations decrease first with $\sqrt{t}$, later exponentially. The resulting concentrations in the groundwater are much lower than saturation; depending on the size of the source, concentrations lower than legal limits may be reached in the groundwater relatively fast.	
Enhanced contaminant removal	1. Increase of temperature (approx. factor 2 per 10°C). 2. Reduction of the effective diffusion distance (size reduction of aggregates or grains).	
Residual NAPL		
Time scale for dissolution of NAPL blobs/ganglia from smear zones	**1 - > 10 years**	**10 - > 100 years**
Time scale for the dissolution of NAPL pools	**> 10 - 1000 years**	**> 1000 years**
Change of release rates / concentrations with time	Dissolution rates are constant over extended periods of time. Locally the concentrations are far above the legal limit (saturation concentrations in the boundary layer to the NAPL).	
Enhanced in-situ decontamination *	1. Increase of the flow velocity. 2. Cosolvent (alcohol) or surfactant flushing for the mobilization and solubilization of residual NAPL.	

* this requires the knowledge of the exact location of the NAPL source

---

[1] Parts of this chapter come from the book: Diffusion in Natural Porous Media: Contaminant Transport, Sorption/Desorption and Dissolution Kinetics. Kluwer Academic Publishers, Boston, 224 p. (ISBN 0-7923-8102-5); Peter Grathwohl (1998)

2.   FILM DIFFUSION

### 2.1   BOUNDARY LAYERS – SHERWOOD NUMBERS

The dissolution rate F_b of NAPL trapped as blobs or ganglia (or pools) in a porous medium (e.g., an aquifer) is limited by diffusion across the NAPL/water interface through an aqueous boundary layer of thickness δ (Fig. 2.1a; Fick's 1st law):

$$F_b = \frac{D_{aq}}{\delta} A \, (C_o - C) \tag{2.1}$$

D_{aq} is the aqueous diffusion coefficient. C and C_o denote the solute concentrations in the mobile (i.e., aqueous) phase and at the interface, respectively. For pure organic liquids and water, C_o is the water solubility (for mixtures see Raoult's law). The ratio D_{aq}/δ is the mass transfer coefficient k [e.g., m s^{-1}]. The overall dissolution rate depends on the surface area (A) of the NAPL available for mass transfer. Often specific surface areas are employed which for example yield the flux per unit volume porous media. For spherical blobs trapped per unit volume in the porous medium the specific surface area then is:

$$A_o = \frac{3 \, \theta_o}{r_b} \tag{2.2}$$

A_o is the area per unit volume porous media (m^2 m^{-3} = m^{-1}). θ_o denotes the NAPL occupied porosity per unit volume of porous medium and r_b the blob radius. θ_o can be calculated from the NAPL saturation ($S°$) and the porosity ($\theta_o = S° \, n$). For $S° = 0.05$ (5%), a porosity of 30% and an effective "blob" radius of 1 mm, the specific interfacial area (A_o) is 45 m^2 m^{-3}. Specific surface areas may be normalized to different reference volumes (pore volume or NAPL volume) and care should be taken to select the right one. In some cases (e.g., mineral dissolution), the overall surface area may not be completely accessible for mass transfer into the flowing water and reduced effective interfacial areas are sometimes used.
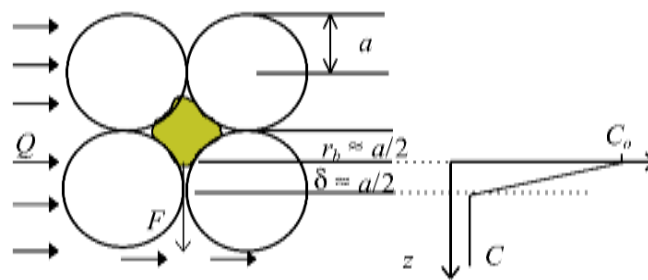
Fig. 2.1: Simplified scheme of dissolution of a NAPL blob (shaded - yellow) by film diffusion (a: grain radius; r_b: radius of blob trapped in pore; δ: effective thickness of an aqueous boundary layer "film")

Since the film thickness depends on the flow velocity and is not explicitly known, k is calculated from empirical relationships, which use a dimensionless constant, the Sherwood number. The Sherwood number Sh is known from various applications in chemical engineering, and for porous media is defined as:

$$Sh = \frac{k\,d}{D_{aq}} = \frac{d}{\delta} \tag{2.3}$$

d denotes here the characteristic length in the porous medium, e.g., the grain size. According to Eq. 2.3, Sh may be interpreted as the ratio between grain diameter and film thickness δ ($k = D_{aq}/\delta$). Sh depends on flow velocity, porosity, and viscosity of water. Various empirical relationships have been developed for the calculation of Sh, e.g., in terms of other dimensionless numbers such as the Schmidt number Sc and the Reynolds number Re. Fitzer et al. (1995) report the following correlation for laminar flow in packed beds:

$$Sh = 1.9\,Sc^{1/3}Re^{1/2} \tag{2.4}$$

The Schmidt number Sc denotes the ratio between the kinematic viscosity (μ) of water and the aqueous diffusion coefficient ($Sc = \mu / D_{aq}$). In groundwater, Sc is for many hydrophobic organic compounds is almost a constant (e.g., $Sc = 2600$ at 10°C; $\mu = 1.3$ x 10^{-6} m^2 s^{-1}; D_{aq} = ca. 0.5 x 10^{-9} m^2 s^{-1}). The Reynolds number in porous media is based on the grain diameter (d), the flow velocity (v_a), and the viscosity μ ($R_e = d\,v_a / \mu$). In natural porous media (aquifers), Re is in most cases less than 1 (e.g.: $v_a = 2$ m d^{-1} and $d = 2$ mm $\Rightarrow Re = 0.36$ and Sh according to Eq. 2.4 approx. 5; in this case δ would be about 1/5 of the grain diameter as shown in Fig. 2.1). Other correlations were investigated for the dissolution of solvents in sands (e.g., Miller et al., 1990; Powers et al., 1991). Powers et al. (1994), for example, found the following relationship in column experiments for the dissolution of naphthalene spheres:

$$Sh = 36.8\,Re^{0.654} \tag{2.5}$$

In this case, the Schmidt number is not used explicitly (for $Re = 0.036$, this correlation results in $Sh = 4.2$, which compares reasonably well with the example above, Eq. 2.4). Note, that a large number of theoretical and empirical Sherwood relationships exist in literature. Liu et al. (2014) reports an elegant correlation for Sherwood numbers for the dissolution of NAPL residuals in porous media, which is only based on the Peclet number (= the product of Re and Sc) as shown in Fig 2.2. This applies if the viscosity of the fluid does not play a major role, and if flow conditions are laminar (typically for groundwater flow). Also, notice that we get a similar solution for the dissolution of DNAPL pools, which is based on boundary layer theory (and some simplifying assumptions).
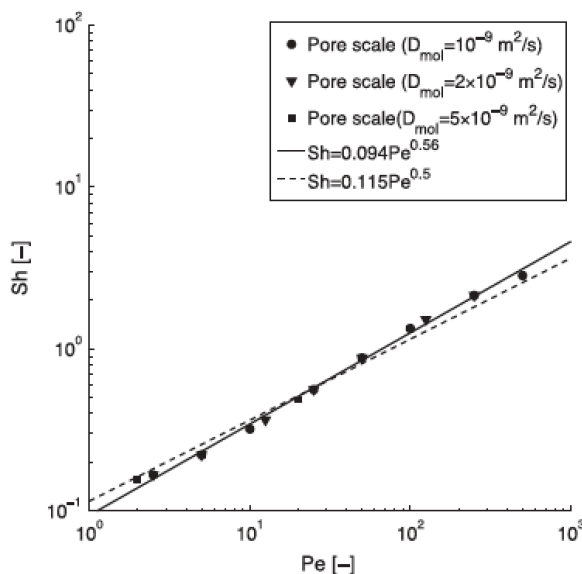
Fig. 2.2: Relationship between Sherwood number (Sh) and Peclet number (Pe) for mass transfer of compounds with different molecular diffusion coefficients in water (from Liu et al., 2014). $Sh = k\,d/D_{aq}$ and $Pe = v_a\,d/D_{aq}$.

For the calculation of the dissolution rates, the specific surface area A_o is required, which, however, is not well known and difficult to determine. Therefore, a modified Sherwood Sh' number was introduced, which also accounts for A_o:

$$Sh' = \frac{kA_o d^2}{D_{aq}}$$

(2.6)

Miller et al. (1990) found the following empirical correlation between Re and Sh' for the dissolution of NAPL in column experiments:

$$Sh' = 12\, Re^{0.75}\theta^{0.6}Sc^{0.5}$$

(2.7)

Using a value of 2,600 for Sc yields Sh' = 612 $Re^{0.75}$ $\theta^{0.6}$. Imhoff et al. (1993) report the following correlation:

$$Sh' = 150\, Re^{0.87}\theta^{0.79}$$

(2.8)

Further and similar empirical correlations are reported in Mayer and Miller (1996) and Imhoff and Miller (1996). It should be noted that these relationships were measured for specific porous media and NAPLs and are not necessarily valid for other systems. However, as shown in Fig. 2.4 mass transfer during the dissolution of NAPL droplets in many cases is fast, and local equilibrium conditions can be assumed at the field scale.

Box 2.1: Boundary layers

The boundary layer approach to describe mass transfer between phases is based on the analogy between mass- and momentum transport in the fluid boundary layer at the interface. This approach originally has been successfully used in heat transfer (see Bennett and Myers, 2008: Momentum, Heat, and Mass Transfer, McGraw-Hill, 3rd ed.).

The boundary layer theory can be applied to the flow of fluids with high viscosity (e.g., water) at low velocity (laminar flow) through flow channels characterized by small characteristic dimensions (i.e., groundwater flow, fixed bed adsorption processes, packed-bed contactors). The boundary layer analogy presumes that the velocity and concentration profiles in the boundary layer are similar in shape, and the mass transport rate is proportional to the momentum transfer rate.
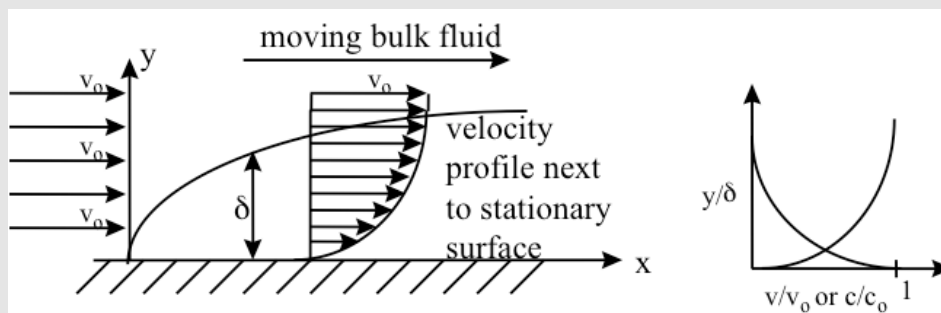
Friction/shear between the moving fluid and the surface causes the velocity of the streamlines (v_o) to decrease as we approach the surface. The resulting velocity and concentration profile are similar (right).

For estimation of the boundary layer thickness (δ) the Sherwood number is frequently used which relates the mass transfer coefficient (k) to the aqueous diffusion coefficient (D_{aq}) and size (d):

$$Sh = \frac{k\, d}{D_{aq}} = \frac{d}{\delta}$$

Sh may be estimated by empirical relationships based on the Reynolds and Schmidt numbers:

$$Sh \sim Re^{1/2}Sc^{1/3}$$

$$Re = \frac{v_a\, d}{\mu}, \ \ Sc = \frac{\mu}{D_{aq}} = \frac{\delta_{hydrodynamic}}{\delta_{concentration}}$$

Re (Reynolds number) represents the ratio of inertial to viscous forces (i.e., dynamic pressure vs. shearing stress), and it is a quantitative indicator of the amount of turbulence in the boundary layer. The boundary layer theory approximation is valid for $0 < Re < 3 \times 10^5$ (v_a: mean or average velocity, d: characteristic length, e.g. grain diameter; μ: kinematic viscosity = dynamic viscosity/density, typically 1×10^{-6} m^2 s^{-1}).

Sc (Schmidt number) represents the ratio of kinematic viscosity to molecular diffusivity (D_{aq}: aqueous diffusion coefficient). This ratio accounts for differences between the diffusivities of solutes, as well as adjusting for the differences between the thickness of the velocity and the concentration profiles (it physically relates the relative thickness of the hydrodynamic layer to the mass-transfer boundary layer).

2.2   LENGTHS OF MASS TRANSFER ZONES

Whether mass transfer limitations must be considered or not depends on the degree of equilibrium achieved if water flows through a mass transfer zone (e.g., consisting of interfaces water / residual NAPL or just water/solids, e.g., during the dissolution of minerals). For external mass transfer resistance (e.g., film diffusion in the aqueous boundary layer surrounding NAPL droplets or crystallites) Fick's first law applies (extended from Eq. 2.1):

$$F' = \frac{D_{aq}}{\delta} A_o \left(C_{w,eq} - C_w \right) \tag{2.9}$$

which simply states that mass transfer occurs by molecular diffusion across a specific interfacial area A_o and a characteristic distance δ (film thickness). F' denotes the flux per unit volume of porous medium. $C_{w,eq}$ is the equilibrium concentration at the interface (water / NAPL or water / solid) and C_w is the concentration in the bulk water at time t, which eventually will reach $C_{w,eq}$. The specific surface area A_o can be calculated from the porosity (n) and the degree of saturation of the pore space with NAPL (S°) yielding the volume of NAPL per unit volume of porous medium (dividing the NAPL volume by the volume of a single spherical blob of NAPL gives the number of NAPL spheres and multiplication by the surface area of one sphere finally yields the specific surface area A_o per unit volume of porous media (in m^2 m^{-3}):

$$F' = \frac{D_{aq}}{\delta} \frac{nS^o 4\pi r^2}{\frac{4}{3}\pi r^3} \left(C_{w,eq} - C_w \right)$$

$$F' = \frac{D_{aq}}{\delta} \frac{nS^o 3}{r_b} \left(C_{w,eq} - C_w \right) = k\, A_o \left(C_{w,eq} - C_w \right) \tag{2.10}$$

k is the mass transfer coefficient (= D_{aq}/δ [m s^{-1}]) and k times A_o denotes a rate coefficient [s^{-1}]. In a water volume traveling through a NAPL contaminated zone, C_w increases with time (or distance at constant velocity) and finally approaches the equilibrium concentration $C_{w,eq}$. Thus, the dissolution rate changes with time and introducing the water-filled pore volume yields the temporal change in concentration:

$$\frac{d\,C_w}{d\,t} = \frac{F'}{n_e} = k\frac{A_o}{n_e}\left(C_{w,eq} - C_w\right) = k\frac{nS^o3}{n_e r_b}\left(C_{w,eq} - C_w\right) \tag{2.11}$$

n_e is the water-filled porosity, which is the total porosity n minus the NAPL filled porosity $(n - n\,S^o)$. A_o/n_e is a specific surface area per volume of pore water (sometimes denoted as A^o). $n\,S^o/n_e$ is the NAPL/water volumetric ratio. If S^o is low (as often the case), the difference between n_e and n is negligible, and A_o/n_e simply is $3\,S^o/r_b$.
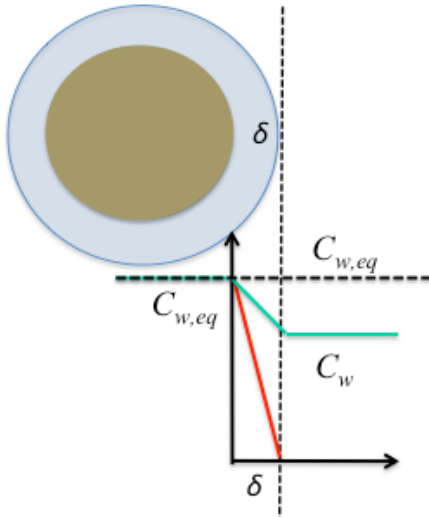
Fig. 2.3: Film diffusion and gradients during the mass transfer of a solute form a droplet of NAPL (or a mineral) across a characteristic distance δ with time into a finite bath; red, green line: initial, intermediate concentration gradient; dashed line: equilibrium conditions establish after a particular time or transport distance (and no net mass transfer occurs anymore).

In a flow-through system (groundwater or column percolation), the change of concentration with distance is relevant, and we may replace t by x/v_a (if the water travels with constant velocity):

$$v\frac{d\,C_w}{d\,x} = \frac{d\,C_w}{d\,t} = k\frac{A_o}{n_e}\left(C_{w,eq} - C_w\right) => \frac{d\,C_w}{d\,x} = \frac{k\,A_o}{v_a n_e}\left(C_{w,eq} - C_w\right) \tag{2.12}$$

which upon integration yields a simple analytical solution for the change of concentration with distance traveled:

$$\int_0^{C_w} \frac{d\,C_w}{C_{w,eq} - C_w} = \int_0^{x} \frac{k\,A_o}{n_e v_a}dx$$

$$-\ln\left(C_{w,eq} - C_w\right) + \ln\left(C_{w,eq}\right) = -\ln\left(1 - \frac{C_w}{C_{w,eq}}\right) = \frac{k\,A_o}{n_e v_a}x \tag{2.13}$$

$$\frac{C_w}{C_{w,eq}} = 1 - \exp\left(-\frac{k\,A_o}{n_e}\frac{x}{v_a}\right)$$

The length of mass transfer zone is defined for an argument of the exponential function of -1, and thus yields for $C_w/C_{w,eq} = 0.632$ ($= 1 - \exp(-1)$):

$$X_s = \frac{v_a n_e}{k\,A_o} = \frac{v_a n_e r_b}{k\,n\,S^o3} \tag{2.14}$$

This may also be easily derived from initial fluxes ($C_w = 0$), and calculating the transport distance needed to achieve $C_{w,eq}$ in water based on eq. 2.12. If n_e is close to n (which often is the case as $S°$ is often lower than 5%) eq. 2.14 reduces to:
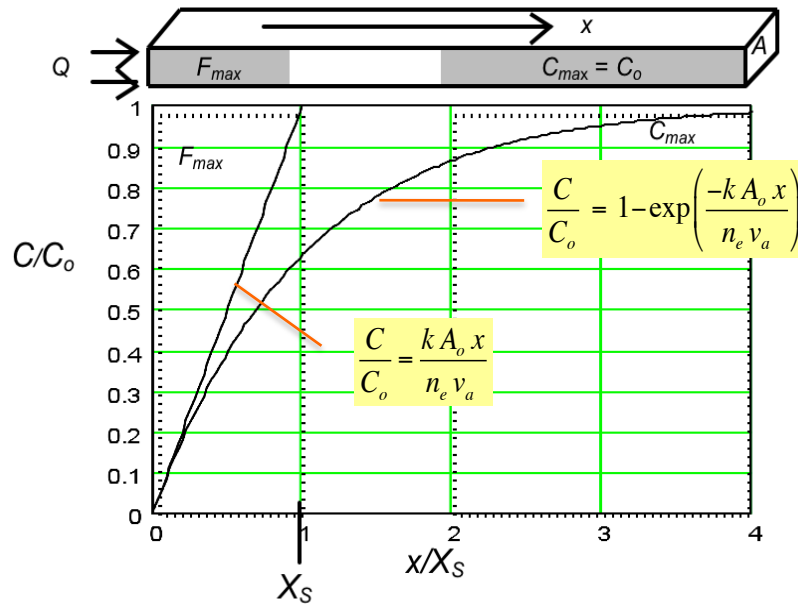
$$X_s \approx \frac{v_a r_b}{3\ k\ S^o} = \frac{2\ v_a\ r_b^2}{3\ Sh\ D_{aq}\ S^o} \qquad (2.15)$$

If a fixed Sherwood number is used to estimate k ($k = Sh\ D_{aq}\ /(2\ r_b)$), then X_s depends on the square of the grain or blob size. Since Sh depends as well on the grain size, different relationships between the X_s and r_b may be obtained (e.g., $X_s \propto r_b^{3/2}$, see Fig. 2.2).
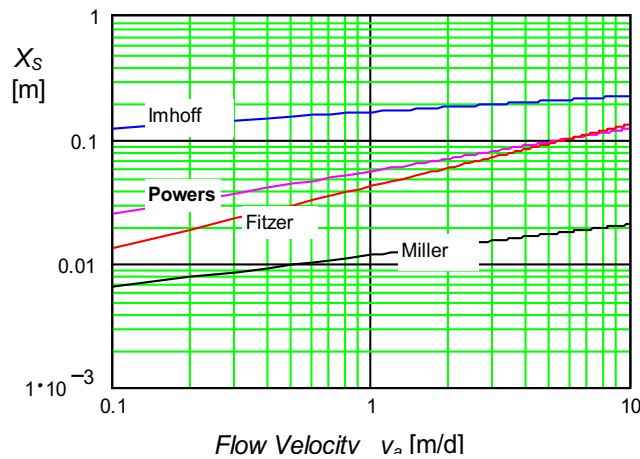
Note that the dissolution of minerals in a packed bed (for easily soluble calcite or gypsum crystals) may be described by the same approach using the volume of the solids (per unit volume) $(1 - n)$ and assuming the total pore volume occupied by water. X_s, in this case, is $v_a\ n\ r\ /(3\ k\ (1 - n))$. X_s may be considered as the "saturation length" as used, e.g., for the description of the dissolution kinetics of carbonate sand by Schulz (1988). X_S is independent of the solubility of the compound ($C_{w,eq}$ or C_o) but varies significantly according to k and A_o. The definitions of k and A_o depend on the governing process (NAPL dissolution or desorption). For barely soluble minerals, intracrystalline processes are limiting and not the aqueous boundary layer.

At $x = X_S$, the contaminant or solute concentration in the groundwater reaches 63.2% of the equilibrium concentration ($C/C_o = 0.632$) as shown in Fig. 2.3. At distances less than X_{Si}, contaminant release occurs at maximum rates (F_{max}). At larger distances ($x >> X_S$), the maximum contaminant concentration ($C_o = C_{w,eq}$) is reached in the groundwater.

Fig. 2.4 shows X_S calculated as a function of the groundwater flow velocity based on various empirical Sherwood correlations from the literature. Although significant differences between the published relationships are obvious, X_S is typically less than one meter in all cases, and for flow velocities below 1 m/d, even less than 10 cm. In laboratory experiments on dissolution kinetics, X_S was observed in the range of 1 cm - 2 cm (Imhoff et al., 1996), < 14 cm (Powers et al., 1994), and < 10 cm (Geller and Hunt, 1993). In heterogeneous sediments, where the distribution of the residual NAPL is highly variable, the length of the mass transfer zone may be larger than in 1D column experiments due to "dissolution fingering" (Mayer and Miller, 1996; Imhoff and Miller, 1996; Imhoff et al., 1996). In some cases, NAPLs may wet the surfaces of the grains and A_o then is given by the surface area of the oil-wet grains. Since this is much larger than A_o for blobs in residual phase, fast dissolution kinetics are expected, resulting in short X_s.

The figure shows a contaminated zone with flow direction x, F_{max} and $C_{max} = C_o$ regions, with equations:

$$\frac{C}{C_o} = 1 - \exp\left(\frac{-k\, A_o\, x}{n_e\, v_a}\right)$$

$$\frac{C}{C_o} = \frac{k\, A_o\, x}{n_e\, v_a}$$

Plot of C/C_o versus x/X_S.

Fig. 2.4: Increase of C/C_o in a contaminated zone. Initially, the contaminant release occurs at maximum flux. After a certain distance, the concentration gradient levels off and equilibrium conditions (maximum concentration) are reached. X_S denotes the length of the mass transfer zone.

Plot of X_S [m] versus Flow Velocity v_a [m/d] showing curves labeled Imhoff, Powers, Fitzer, Miller.

Fig. 2.5: Comparison of different empirical correlations for the calculation of X_S based on the Sherwood number: Miller et al., 1990; Imhoff et al. (1993); Powers (1994); Fitzer et al. (1995); all calculations based on: $d = 2$ mm; $r_b = d/4$; $\theta = 0.35 \cdot 0.05 = 0.0175 \Rightarrow A_o = 105$ m^2 /m^3; $n_e = 0.35 - \theta = 0.3325$; .

2.3   DISSOLUTION OF NAPL POOLS

As NAPLs infiltrate into the subsurface, they may encounter less permeable strata, which act as capillary barriers impeding further vertical movement, or they may reach the base of the aquifer. The result is the formation of a coherent lateral body of the NAPL phase, a "pool," e.g., at the bottom of the aquifer. The contaminant release rates out of NAPL pools depend on the contact time between the aqueous phase and the contaminated region. Due to the less favorable surface/volume ratio, pools dissolve slower than dispersed residual phase (blobs).

The dissolution behavior of pools can be calculated assuming that dissolution occurs due to diffusion and transverse vertical dispersion of the NAPL constituent(s) according to Fick's 2nd law.

8

The concentration profile which develops as the groundwater passes the pool can be calculated using the analytical solution for the semi-infinite case and a constant source (Hunt et al., 1988; Johnson and Pankow, 1992):

$$\frac{C}{C_o} = \text{erfc}\left(\frac{z}{2\sqrt{D\frac{x}{v_a}}}\right) \quad (2.16)$$

x/v_a represents the residence time of the groundwater in contact with the pool. v_a is the groundwater flow velocity parallel to the pool. For a pool of length L_p, the contact time t_c equals L_p/v_a. z denotes the vertical distance above the pool. D accounts for the diffusion and transverse vertical dispersion coefficient [L^2 s^{-1}]:

$$D = D_p + \alpha_t v_a \quad (2.17)$$

α_t and D_p denote the transverse dispersivity [L] and the pore diffusion coefficient [L^2 t^{-1}] in the aquifer (in a first approximation D_{aq} times porosity), respectively.
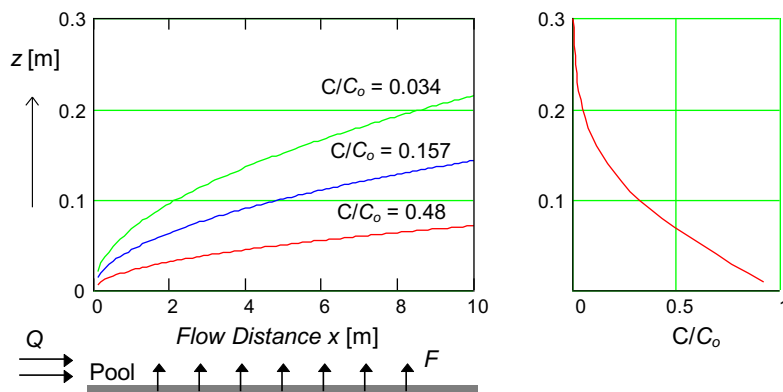
Fig. 2.6: Isolines of relative concentrations (left) and the concentration profile developed downgradient of a pool (groundwater flow velocity 1 m/d; D_p = 1.75 x 10^{-10} m^2/s; α_t = 0.5 mm) which close to the pool surface decreases linearly in vertical direction (right).
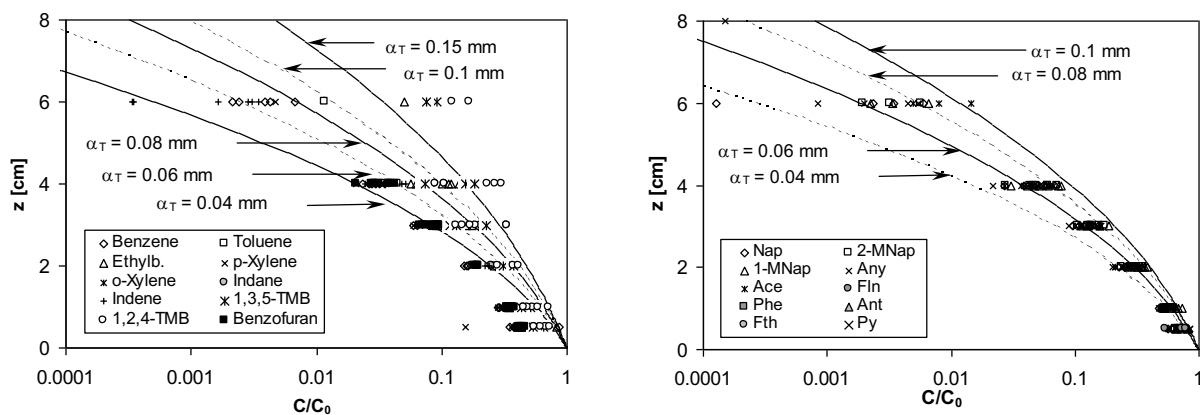

Fig. 2.7: Concentration profiles measured for different compounds (BTEX: left, PAHs: right) 5 cm before the end of a 2.5 m long coal tar pool compared to profiles calculated with different values for α_t and eq. 2.16; flow velocity: 1.7 m d^{-1} (Eberhard and Grathwohl, 2002).

Box 2.3: Mixing cell model for dispersion dominated pool dissolution (Loyek, 1998)

The porous medium is assumed as a (3D) tetrahedral packing of spheres; flow is from left to right, and at the lower boundary (interface to the pool surface), the equilibrium concentration is applied (pool as an infinite source). Mixing is assumed as complete in the pore throats. The distance of the mixing cells (pore throats) in the flow direction (x) and perpendicular (z) to that is the one-grain radius ($r = 1$). "Steady-state" conditions are assumed ($dC/dt = 0$). The number of mixing cells (MZ) in the flow direction, in this case, depends on the length of the pool l_p, and the grain radius (r_a):

$$MZ = \frac{l_p}{1 r_a}$$
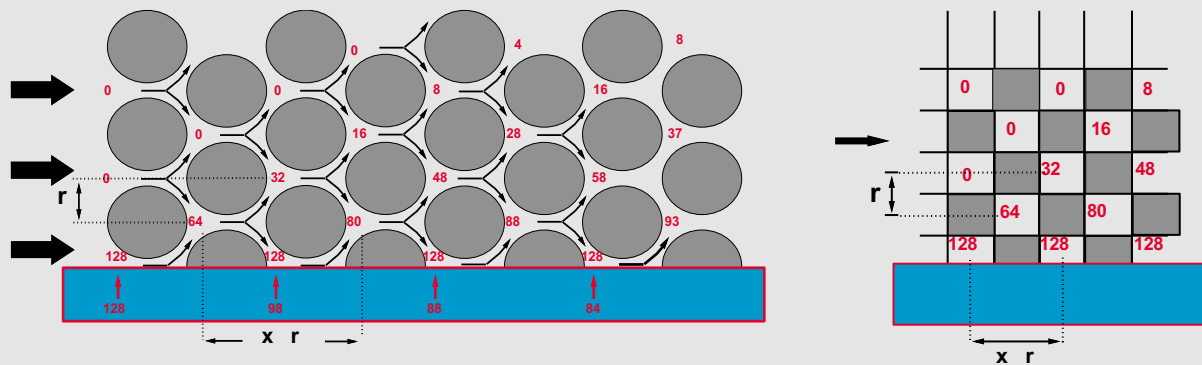
Scheme of mass transfer from the pool surface assuming complete mixing in the pore throats. Numbers indicate the distribution of particles in the porous medium (at the right-hand side calculated in an Excel spreadsheet). At the interface, the equilibrium concentration ($c_{i,w}^{sat}$) of 400 (particles) is assumed.

$$\frac{c_i^w(l_p, z)}{c_i^{w,sat}} = \mathrm{erfc}\,\frac{z/r_a}{2\sqrt{0.5\,MZ}}$$

$$= \mathrm{erfc}\,\frac{z}{2\sqrt{0.5\,r_a\,l_p}}$$

$$\approx \mathrm{erfc}\,\frac{z}{2\sqrt{\alpha_t\,l_p}}$$
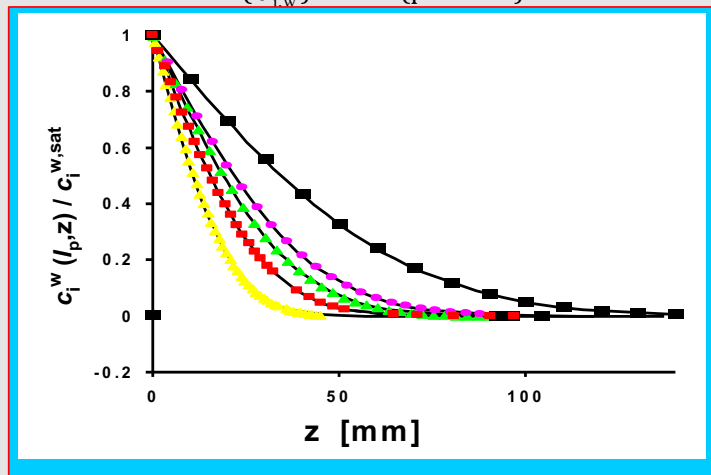
Displayed above are concentration profiles at the end of a pool (90 cm long) for different grain radii (r_a) in a porous medium. Symbols denote the concentrations calculated with the mixing-model (Excel); lines were calculated with the analytical solution of Ficks 2nd law (erfc). Note that the concentration profile is independent of the flow velocity, and α_t is a function of the grain radius ($\alpha_t = 0.5\,r_a$).

Pool dissolution rates. The mass, which has diffused into the groundwater while in contact with the pool is:

$$M = 2\, C_o n \sqrt{\frac{D\, t_c}{\pi}}\, L_p B_p \tag{2.18}$$

C_o denotes the equilibrium concentration of the solute at the interface between pool and groundwater, i.e., is the solubility of a pure compound or the equilibrium aqueous concentration according to Raoult's law for an organic mixture. B_p is the width of a representative cross-section of the pool (e.g., a central strip, 1 m wide through the center of the pool). t_c is the contact time (= L_p/v_a). The overall dissolution rate of a pool of length L_p is:

$$F_p = 2C_o n \sqrt{\frac{D}{\pi\, t_c}}\, L_p\, B_p = 2C_o n \sqrt{\frac{D}{\pi\,\frac{L_p}{v_a}}}\, L_p\, B_p = 2C_o n \sqrt{\frac{DL_p v_a}{\pi}}\, B_p \tag{2.19}$$

Much simpler is the calculation of the dissolution rate based on other "equivalent" models from the boundary theory, as described below.

Equivalent models. Other models that assume film diffusion (Fick's 1st law) or a groundwater layer of a given height saturated with the solute (see Fig.) may be considered as alternatives to the semi-infinite diffusion/dispersion model for the prediction of the dissolution kinetics of pools. Eq. 2.18 can be written equivalently to Fick's 1st law, allowing the calculation of the effective film thickness:

$$F_p = D\, n\, \frac{C_o}{\delta}\, L_p\, B_p \implies \delta = \sqrt{Dt_c\, \frac{\pi}{4}} \tag{2.20}$$

Similarly, the thickness of a layer of water that is saturated with the solute can be calculated based on the pool dissolution rate (Eq. 2.18) and the groundwater flow rate in that layer ($Q = B_p\, Z_S\, v_a\, n$). In essence, the "saturation height" Z_S is:

$$C = \frac{F_p}{Q} = \frac{2\, C_o\, n \sqrt{\frac{D\, L_p\, v_a}{\pi}}\, B_p}{v_a\, n\, B_p\, Z_s}$$

$$\implies \quad Z_s = \frac{2C_o \sqrt{\frac{D\, L_p\, v_a}{\pi}}}{C_o\, v_a} = \sqrt{D\, t_c\, \frac{4}{\pi}} \tag{2.21}$$

In both cases δ and Z_S are close to the square root of the mean square displacement ($z^2 = D\, t_c$):

$$Z_s = \sqrt{Dt_c}\, \sqrt{4/\pi}\, ; \; \delta = \sqrt{Dt_c}\, \sqrt{\pi/4} \tag{2.22}$$

It should be noted that z^2 (and thus also Z_S) depends on the transverse vertical dispersivity, which dominates the dissolution behavior at high flow velocities and/or high values of α_t. If ($\alpha_t \cdot v_a$) is much higher than D_p, z^2 becomes independent of the flow velocity ($z^2 = D\, t_c = (D_p + \alpha_t\, v_a)\, L_p/v_a$; for $\alpha_t\, v_a \gg D_p$: $z^2 = \alpha_t\, L_p$) and Z_S depends only on α_t and the length of the pool.

$$Z_s \approx \delta \approx \sqrt{\alpha_t\, L_p} \tag{2.23}$$

If $(\alpha_t\, v_a)$ is large compared to the pore diffusion coefficient, the dissolution rate becomes directly proportional to the flow velocity (Fig. 2.9).
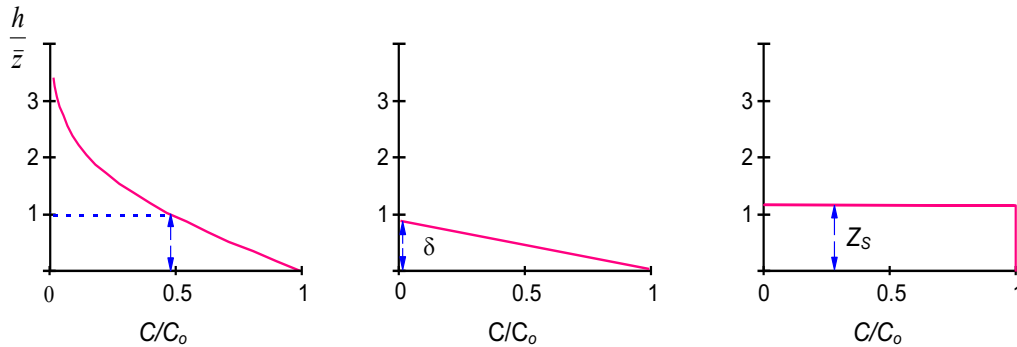
Fig. 2.8: Equivalent models for the calculation of the dissolution rates from NAPL pools (left: semi-infinite diffusion, $\bar{z}$ = mean square displacement $(\alpha_t\, x)^{0.5}$; middle: Fick's 1st law, δ: film thickness $(= (\pi/4\; \alpha_t\, x)^{0.5})$; right: saturation concentration C_o within a "boundary" layer of height $Z_S = (4/\pi\; \alpha_t\, x)^{0.5}$.
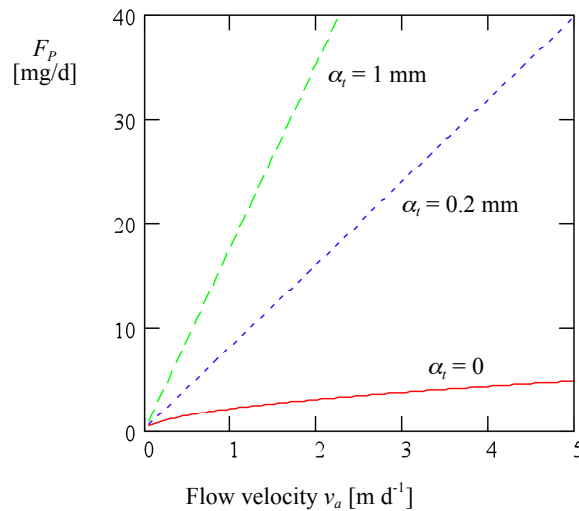
Fig. 2.9: Dependency of the pool dissolution rate F_p (2 m long and 1 m wide) on the flow velocity with different values of transverse vertical dispersivity (α_t); D_p = 1,75 x 10^{-10} m^2 s^{-1}; C_o = 1 mg L^{-1} (at higher solubilities the dissolution rates increase correspondingly).

Box 2.4: Transverse dispersion coefficients - dispersivities

The local transverse dispersivity α_t is much smaller than the longitudinal dispersivity (which, to a large extent, comes from differential advection) and more than one order of magnitude smaller than the mean grain size. The diagram shows vertical transverse dispersivities α_t at various flow velocities. A decrease with increasing flow velocity occurs, indicating incomplete mixing at pore throats (all data were obtained in fully saturated media, except the data from Susset (1998) and Klenk (2000) which result from transport across the capillary fringe (Klenk and Grathwohl, 2002). The apparent decline of transverse dispersivities leads to a nonlinear empirical correlation to estimate the transverse dispersion coefficient based on the Peclet number (Pe):
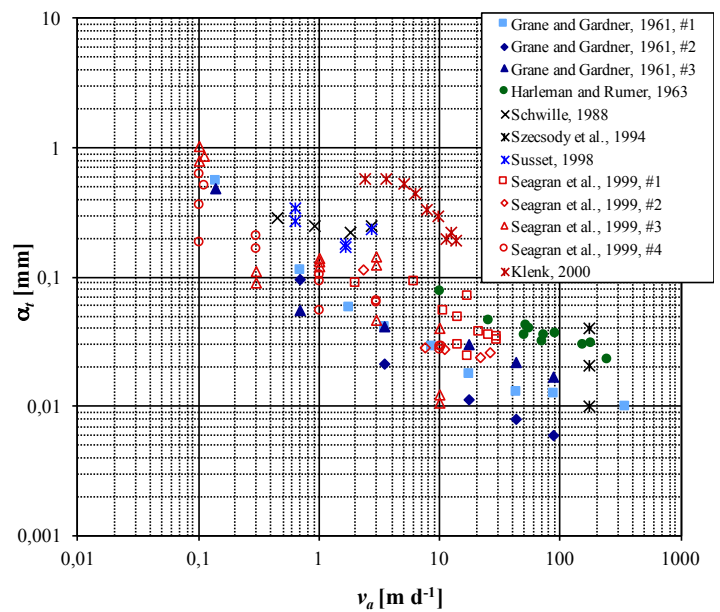
$$Pe = \frac{v_a d}{D_{aq}}$$

$$\frac{D_t}{D_{aq}} = \frac{3}{2}\left(\frac{4}{\pi}Pe\right)^{0.5} \text{ (mass transfer across the capillary fringe: Klenk and Grathwohl, 2001)}$$

$$\frac{D_t}{D_{aq}} = \frac{D_p}{D_{aq}} + 0.28(Pe)^{0.72} \text{ (tracer experiments fully saturated: Olsson and Grathwohl, 2006)}$$

$$\frac{D_t}{D_{aq}} = \frac{D_p}{D_{aq}} + \sqrt{\frac{Pe^2}{Pe + 2 + 4 + 5.5^2}} \Rightarrow D_t = D_p + v_a\frac{d}{\sqrt{Pe + 123}} \text{ (Chiogna et al., 2010)}$$

Comparison of empirical equations for prediction of D_t based on the Peclet number (Pe):
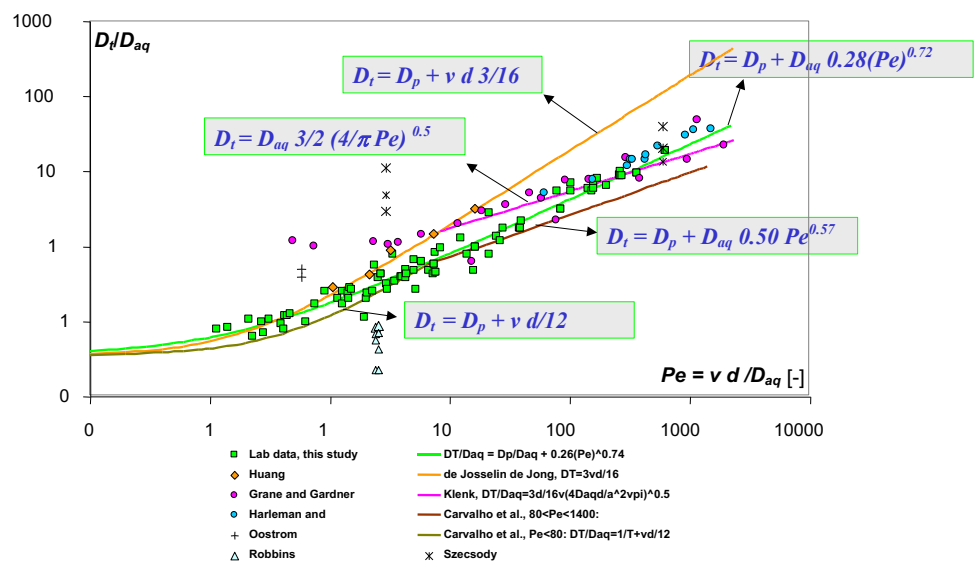
Box 2.5: Film thicknesses

Note the similarity of the relationships obtained for pool dissolution with empirical correlations to estimate Sherwood numbers, e.g., from Liu et al. (2014) who report $Sh = 0.1 \, (Pe)^{1/2}$ for pore-scale dissolution of residual NAPL

$$\delta = \frac{d}{Sh} = \frac{d}{0.1\sqrt{Pe}} = \frac{d}{0.1\sqrt{\dfrac{v\,d}{D_{aq}}}} = 10\sqrt{\frac{D_{aq}d}{v_a}}$$

which is similar to the expression we get for the boundary layer thickness in pool dissolution, e.g., eq. 2.21, assuming that at the pore-scale D_t is replaced by D_{aq} and the length of the pool represents the grain size:

$$\delta = \sqrt{\frac{\pi}{4}\frac{D_t L_{pool}}{v_a}} \cong \sqrt{\frac{D_{aq}\,d}{v_a}}$$

The discrepancy of these two approaches (i.e., factor 10) reflects the uncertainty in using empirical relationships for different scenarios (pore-scale *vs*. large scale). If we take, e.g., the classical Fitzer relationship, then the film thickness becomes:

$$\delta = \frac{d}{Sh} = \frac{d}{1.9 Re^{1/2} Sc^{1/3}} = \frac{d}{1.9\left(\dfrac{dv_a}{\mu}\right)^{1/2}\left(\dfrac{\mu}{D_{aq}}\right)^{1/3}} = \frac{\sqrt{\dfrac{d\,\mu}{v_a}}}{1.9\left(\dfrac{\mu}{D_{aq}}\right)^{1/3}} \cong 0.5\sqrt{\frac{D_{aq}d}{v_a}}$$

The approximation is obtained by assuming an empirical exponent of the Schmidt number of ½ (note, the product of $Re \times Sc$ is the Peclet number ($Pe = v_a\,d\,/D_{aq}$). This is similar to pool dissolution but yields very different film thicknesses compared to Liu et al. (2014), as we saw already in Fig. 2.5 comparing different empirical relationships.

3.   ASSESSMENT OF NAPL CONTAMINATED SITES

3.1   DEPTH-AVERAGED CONCENTRATIONS

The most important conclusion for risk assessment from the above discussion is that, in areas which are contaminated by residual NAPL (blobs trapped in the porous media, e.g., a smear zone of oil in the capillary fringe), equilibrium is reached after a short flow distance and the contaminant concentration in the "contact" groundwater is given by the water solubility of the NAPL (for organic mixtures according to Raoult's law, see next session). The depth-averaged contaminant concentration downgradient from a contaminant source is then simply given by the dilution rate. In essence, the thickness of the contaminated zone Z_o compared to the thickness of the aquifer h:

$$C_{avg} = C_o \frac{z_o}{h}$$
(3.1)

For the pool dissolution scenario, z_o is given by the height of the chemical boundary layer Z_s.

3.2   RETARDATION OF CLEAN WATER FRONTS IN SMEAR ZONES

Remediation of subsurface contamination by in situ techniques, such as pump-and-treat methods in the saturated zone or vapor phase extraction for removal of volatile compounds from the unsaturated zone, is most efficient if equilibrium conditions are achieved - high flow rates of water or air result in fast removal of the contaminants. If equilibrium conditions apply for the dissolution of residual NAPLs ("blobs"), then the time scale for remediation can be estimated from the velocity of the dissolution front (v_{Dis}), which is retarded compared to the groundwater flow velocity (v_a). The retardation factor is given by the ratio of the overall mass of contaminant present in the porous medium to the mobile (i.e., dissolved) contaminant:

$$R = \frac{v_a}{v_{Dis}} = \frac{n_e C_o + \rho_o n S^o}{C_o n_e}$$
(3.2)

This retardation factor equals the number of pore volumes, which have to be replaced until the complete dissolution of the NAPL is achieved. ρ_o n S° represents the NAPL mass per unit volume soil, and $n_e C_o$ is the mobile fraction of the contaminant (i.e., dissolved in pore water). ρ_o denotes the density of the organic phase (NAPL, the same unit as C_o e.g., kg m^{-3}), n is the porosity, S^o is the degree of saturation with NAPL) and n_e is effective porosity (= $n - n S°$). Since the solute mass dissolved in the pore water is, in most cases, insignificant compared to the mass of the NAPL, Eq. 3.2 reduces to:

$$R = \frac{\rho_o n S^o}{C_o n_e} = \frac{\rho_o S^o}{C_o}$$
(3.3)

If n_e is close to the overall porosity (n) Eq. 3.3 becomes simply: $R = \rho_o S° /C_o$ (S° is the degree of saturation). As long as equilibrium conditions apply, high flow velocities (e.g., close to a well during application of pump-and-treat techniques) will result in fast dissolution/remediation of residual NAPL (in contrary to non-equilibrium, when diffusion is limiting, then release rates are independent of the groundwater flow velocity).

3.3   TIME FOR DISSOLUTION OF POOLS

The dissolution of NAPL from pools is much slower than the equilibrium dissolution of residual blobs of NAPL (this is due to the much lower interfacial area between NAPL and the mobile water). The time for pool dissolution can easily be calculated from the dissolution rate F_p (based on Z_S) and the mass of NAPL in the pool (assuming that the pool shrinks in height but not in length during dissolution and considering only a rectangular strip in the center of the pool, e.g., 1 m width):

$$t_{Dis} = \frac{M_p}{F_p} = \frac{L_p H_p\,\rho_o n S^o}{C_o v_a n Z_s} \tag{3.4}$$

H_P denotes the pool height (the NAPL saturation $S°$ in the pool is close to 1). Fig. 3.1 shows some example calculations with a value for α_t of 0.1 mm. Even at flow velocities of 1 m/d, the time scale of TCE dissolution from pools is of the order of several decades to a century. Compounds with lower solubilities (C_o) would need even more time to be dissolved from a pool. At slow flow velocities, the dissolution time depends on the square root of v_a, whereas at higher flow velocities, the time for pool dissolution decreases linearly with increasing v_a.
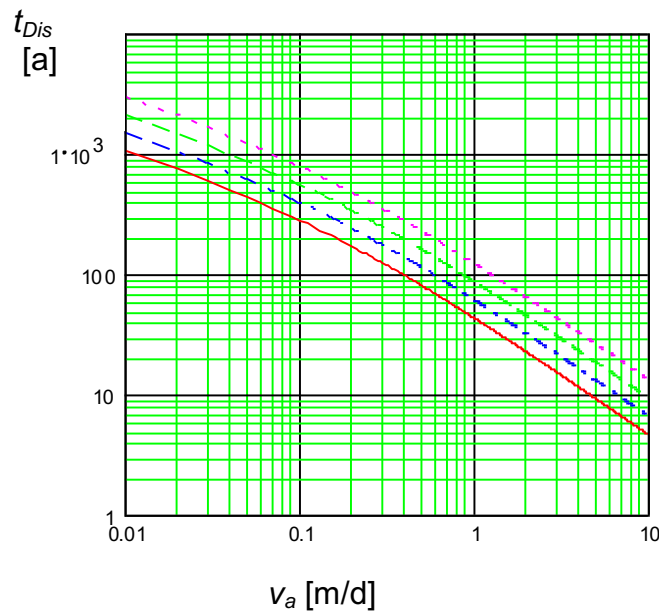
Fig. 3.1: Time scales for dissolution of TCE pools (solid line: pool length = 2 m, 100 kg TCE; dotted line: pool length = 16 m , 800 kg TCE; other lines: pool lengths = 4 m and 8 m, 200 kg and 400 kg TCE, respectively; D_p = 2E-10 m^2 s^{-1}; α_t = 0.1 mm).

Box 3.1: "Stacked" NAPL-pools in heterogeneous porous media

NAPL in the subsurface are usually not uniformly distributed, which means that contaminant concentrations in water show a high special variability. Water in areas containing residual NAPL is near the saturation concentration, while water outside shows low concentrations. Downstream water mixes through transverse dispersion. Various attempts have been made to simulate dissolution from multiple pools in the subsurface. An example is depicted below.
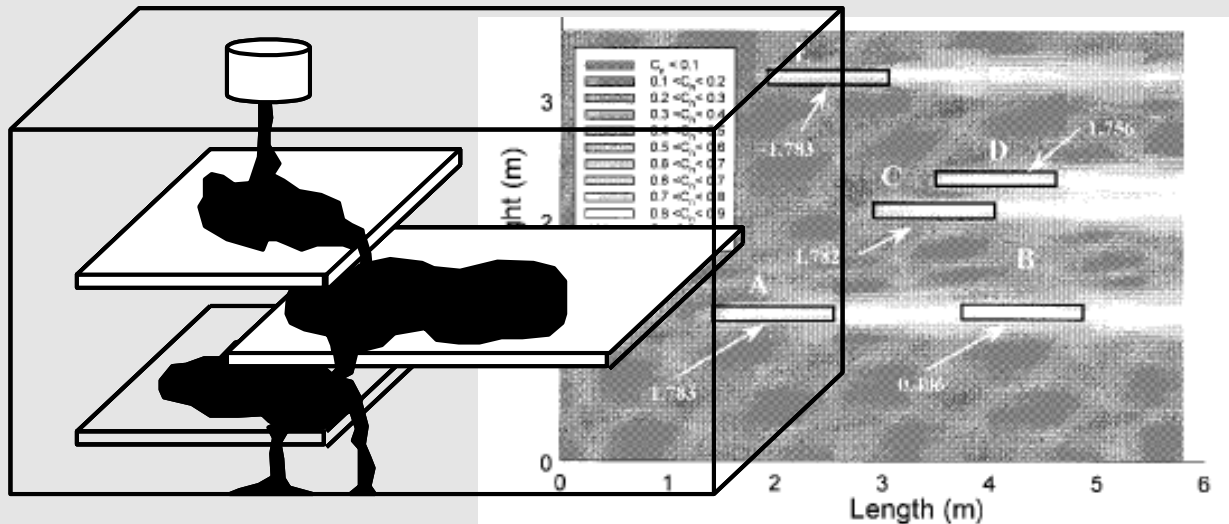
Figure 14. Normalized concentration distribution and mass transfer rates in a multiple subzone source.

More on dissolution and dispersion in heterogeneous porous media in:

Ronald W. Falta, WATER RESOURCES RESEARCH, VOL. 39, NO. 12, 1360, 2003: Modeling sub-grid-block-scale dense nonaqueous phase liquid (DNAPL) pool dissolution using a dual-domain approach

Werth, C. J., O. A. Cirpka, and P. Grathwohl (2006): Enhanced mixing and reaction through flow focusing in heterogeneous porous media, Water Resour. Res., 42 (12), W12414, doi:10.1029/2005WR004511

3.4   TIME FOR DISSOLUTION OF SINGLE SPHERES (OIL DROPLET, GAS BUBBLE, CRYSTAL, ETC.)

The change in mass (M) of a sphere during dissolution (e.g., sugar crystal in tea) depends on the mass transfer coefficient (k), the saturation concentration at the interface (C; often corresponds to the solubility of the material), and the interfacial area (the surface area of a sphere with radius r is: $A = 4 \pi r^2$):

$$\frac{d\,M}{d\,t} = -k\,C\,A$$

$$\frac{d\,M}{d\,t} = -k\,C\,4\,\pi r^2 \quad \text{and with } r = \left(\frac{3M}{4\pi\rho}\right)^{1/3} \tag{3.5}$$

$$\frac{d\,M}{d\,t} = -k\,C\,4\,\pi \left(\frac{3\,M}{4\,\pi\,\rho}\right)^{2/3}$$

ρ denotes the density of the sphere (its "concentration per volume"). The product of $k\,C$ represents the surface area normalized dissolution rate (e.g. in g m^{-2} s^{-1}, if multiplied with the molecular weight in mol m^{-2} s^{-1}), which typically is reported in literature for the dissolution of minerals. Integration from the initial radius r_o to r and for the time from 0 to t yields:

$$\int_{M_o}^{M} \frac{d\,M}{M^{2/3}} = \int_{o}^{t} -kC\,4\pi \left(\frac{3}{4\pi\rho}\right)^{2/3} dt$$

$$3M_o^{1/3} - 3M^{1/3} = 0 + k\,C\,4\,\pi \left(\frac{3}{4\,\pi\,\rho}\right)^{2/3} t \tag{3.6}$$

$$M^{1/3} = M_o^{1/3} - k\,C\,\frac{4}{3}\pi \left(\frac{3}{4\,\pi\,\rho}\right)^{2/3} t$$

with $M = 4/3\,\pi\,r^3\,\rho$ we get the solution for the radius as a function of time:

$$r = r_o - \frac{k\,C}{\rho} t \tag{3.7}$$

From this, the time needed to dissolve the sphere ($r = 0$) can be calculated by:

$$t_{diss} = \frac{r_o\,\rho}{k\,C} \tag{3.8}$$

For comparison, the time needed to dissolve the sphere based on the maximum initial flux (without accounting for the shrinking surface area of the sphere) is three times shorter:

$$\frac{4}{3}\,\pi\,r^3 = k\,C\,4\,\pi\,r^2\,t \quad \Longrightarrow \quad t_{diss} = \frac{r_o\,\rho}{3\,k\,C}\left(= \frac{M_p}{F_p}\right) \tag{3.9}$$

Note the similarity to eq. 3.4.

Accounting for k – size (e.g., $d = 2\,r$) relationships. The mass transfer coefficient (k) depends on the radius (r) in empirical relationships such as the Sherwood number (Sh):

$$k = \frac{D_{aq}}{\delta} \quad \text{and } Sh = \frac{d}{\delta} = \frac{2\,r}{\delta}$$

$$\Rightarrow k = \frac{D_{aq}Sh}{2\,r} \tag{3.10}$$

Solving the mass balance equation directly for the radius we get:

$$d(M) = (-k\, C\, 4\, \pi\, r^2)dt$$

$$d\left(\frac{4}{3}\, \pi\, r^3 \rho\right) = \left(-\frac{D_{aq}Sh}{2\, r}C\, 4\, \pi\, r^2\right)dt \tag{3.11}$$

$$\frac{1}{r}dr^3 = \left(-D_{aq}\frac{3}{2}Sh\frac{C}{\rho}\right)dt$$

Integration (with $r^3 = a$, $r = a^{1/3}$, $r^2 = a^{2/3}$ and re-substitution) yields:

$$\int_{r_o}^{r}\frac{1}{r}dr^3 = \int_{0}^{t}\left(-D_{aq}\frac{3}{2}Sh\frac{C}{\rho}\right)dt$$

$$r_o^2 - r^2 = D_{aq}Sh\frac{C}{\rho}t \tag{3.12}$$

$$r = \sqrt{r_o^2 - D_{aq}Sh\frac{C}{\rho}t}$$

The time to dissolve the sphere in this case is:

$$t_{diss} = \frac{r_o^2 \rho}{D_{aq}\, Sh\, C} \tag{3.13}$$

Thus, at a given Sherwood number (often between 2 and 6), the time to dissolve the sphere increases with the radius squared. Since Sh often is found to be a function of the square root of Re or Pe, the dissolution time scales with the radius to the power of 3/2.

4.   DISSOLUTION OF MIXTURES

4.1   RAOULT'S LAW AND PARTITION COEFFICIENTS

As shown above, the driving force for mass transfer is the concentration at the interface, which depends on the partition coefficient of compound i between the organic mixture and water phase. In complex mixtures of organic compounds (e.g., coal tar, gasoline), the aqueous phase saturation concentration of the individual components $C_{i,w}$ depends on the composition of the mixture (Banerjee, 1984; Mackay et al., 1991; Lane and Loehr, 1992; Lee et al., 1992). $C_{i,w}$ is always less than the solubility of the pure substances in water and can be determined in liquid/liquid mixtures following Raoult's Law (Pyka, 1994; Loyek and Grathwohl, 1995):

$$C_{i,w} = \chi_{i,o}\gamma_{i,o}S_i \tag{4.1}$$

where $C_{i,w}$, $\chi_{i,o}$ and $\gamma_{i,o}$ denote the concentration of component i in water [g l^{-1} or mol l^{-1}]; the molar fraction of component i in the organic mixture [n_i / $\Sigma\, n_i$]; and the activity coefficient of i in the organic mixture (most =1); S_i is the solubility in water of the individual component i (pure substance) in g l^{-1} or mol l^{-1} (for solids of the subcooled liquid, for gases of superheated liquid; or the enhanced solubility in the presence of cosolvents (e.g., alcohols).

The activity coefficient ($\gamma_{i,o}$) describes the deviation from the ideal behavior. For an ideal mixture: $\gamma_{i,o}$ = 1, meaning Eq. 4.1 simplifies to:

$$C_{i,w} = \chi_{i,o}\, S_i \tag{4.2}$$

The molar fraction $\chi_{i,o}$ can have a maximum value of 1 for a pure compound, and can be easily calculated from the mean molecular weight of the mixture (M_o [g mol^{-1}]), the molecular weight of i [g mol^{-1}] and the fraction of i within the mixture ($f_{i,o}$ or weight-%/100):

$$\chi_{i,o} = f_{i,o}\frac{M_o}{M_i}; for\ M_o \cong M_i\ then\ \chi_{i,o} \cong f_{i,o} \tag{4.3}$$

In many cases, M_o/M_i in organic liquids (e.g., fuels) is between 0.5 and 1.5. For the solubility from organic mixtures, the following equation applies:

$$C_{i,w} = f_i\frac{M_o}{M_i}S_i$$

and in the first rough approximation ($M_o/M_i \cong 1$): $\qquad\qquad$ (4.4)

$$C_{i,w} = \frac{weight\%_i}{100}S_i$$

$C_{i,w}$ is always less than the solubility of the pure substance (also when the solubility of the subcooled liquid is higher than the solubility of the solid substance: precipitation of crystals would occur if the solubility of the pure substance is exceeded).

Box 4.1: Partition coefficients between organic mixtures and water

SInce $f_{i,o}$ represents the concentration of i in the organic phase mixture (in kg kg^{-1}), the partitioning coefficient between an organic phase and water ($K_{o/w}$) can be derived from Raoult's Law using:

$$K_{o/w} = \frac{C_{i,o}}{C_{i,w}} = \frac{f_{i,o}}{f_{i,o}\frac{M_o}{M_i}S_i} = \frac{1}{\frac{M_o}{M_i}S_i}$$

The partition coefficient is independent of concentration. For $M_o = M_i$ or a pure solvent (e.g., Toluene in Toluene: $C_{i,o}$ = 1 kg kg^{-1}; $C_{i,w}$ = S_i). The partitioning coefficient between a pure organic phase ("solvent") and water then would be simply: $K_{o/w} \approx \frac{1}{S_i}$ (= "ideal" case)

Box 4.2: Retardation factor of the "clean waterfront" moving through a smear zone of residual phase during the dissolution of a compound form an organic NAPL mixture

How fast the dissolution of a NAPL constituent happens depends on the retardation factor. The retardation factor is defined as:

$$R_d = \frac{total\ concentration}{mobile\ concentration} = \frac{C_{i,w}\ n_e + n\ S^o\ \rho_o\ C_{i,o}}{C_{i,w}\ n_e} = 1 + \frac{C_{i,o}\ n\ S^o\ \rho_o}{C_{i,w}\ n_e}$$

$n\ S°$ represents the oil-filled pore volume [e.g., $m^3\ m^{-3}$], ($n\ S°\ \rho_o$) the mass of oil [kg m^{-3}] and ($n\ S°\ \rho_o\ C_{i,o}$) finally the mass of the compound in the NAPL per volume of porous media [kg of i per m^3]. n_e is the effective water-filled pore volume = $n - n\ S°$ (the pore volume minus the NAPL volume). $C_{i,o}/C_{i,w}$ represents the partition coefficient $K_{o/w}$ (which comes from Raoult's law, as shown in Box 1.1). $n\ S°\ \rho_o$ /n_e is oil to water ratio in the porous media. For a pure NAPL (e.g., pure toluene) $C_{i,w}$ is represented by the water solubility of the compound S_i. Thus, the retardation factor is:

$$R_d = 1 + K_{o/w}\ \frac{n\ S^o\ \rho_o}{n_e} \approx 1 + \frac{n\ S^o\ \rho_o}{\frac{M_o}{M_i}\ S_i\ n_e}$$

As $K_{o/w}$, R_d is independent of the composition of the organic mixture. The term to the right is obtained by implementing Raoult's law with an activity coefficient of 1. Thus, the movement of a clean waterfront through a NAPL smear zone is independent of the solute content in the NAPL, but depends on the amount of NAPL in the porous medium. The equation further simplifies if the molecular weights of the NAPL and compound i are assumed to be similar ($M_o \cong M_i$) and $n_e \cong n$:

$$R_d \cong 1 + \frac{nS^o\rho_o}{S_i n_e} \cong 1 + \frac{S^o\rho_o}{S_i}$$

4.2   DOUBLE FILM DIFFUSION

In NAPL mixtures (e.g., fuels) mass transfer of a constituent may be limited by diffusion in the NAPL and water (or gas phase during volatilization). The double-film diffusion model approximates the NAPL-water interface by introducing two films adjacent to the interface, where one film represents a stagnant water layer and a second layer in the multi-component organic phase (see Fig. 4.1).

The concentration of contaminants across this multi-component organic film decreases from the initial concentrations ($C_{i,o}$) in the organic phase to the concentration at the NAPL-water interface ($C_{i,o/w}$). At the boundary layer between the two films, organic contaminants leave the organic phase and enter the aqueous phase. The concentrations at the NAPL-water interface are at equilibrium and given by the organic-water partition coefficient ($K_{o/w}$) of the respective compounds.

**Org. phase mixture
Tar oil/creosote**

**Water
Mobile Phase**
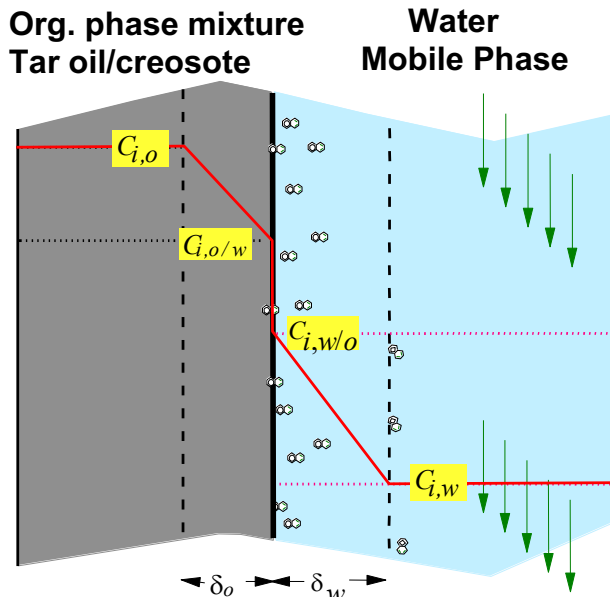
Fig. 4.1: Schematic view of the stagnant two-film model. Mass transfer across both films is assumed to be controlled by Fick's 1st law. At the interface between both films, "local equilibrium" is assumed, and concentrations on either side are controlled by the partition coefficients of the component between the organic phase and water. δ_o and δ_w refer to the respective film thicknesses; $C_{i,o}$ and $C_{i,w}$ are the concentrations in the organic and aqueous phase, respectively.

To calculate the contaminant flux across the two films, the following assumptions have to be made:

o   the concentration in the mobile water is constant (e.g. close to zero if water continuously displaced during remediation): $C_{i,w} = 0$

o   steady-state conditions apply for the flux of contaminant across both layers (no storage)

o   the concentration at the NAPL-water interface ($C_{i,o/w}$) is at equilibrium with the concentration at the water-organic interface ($C_{i,w/o}$) (e.g., saturation concentration in water, according to Raoult's law)

Then, the fluxes in each film can be evaluated using Fick's 1st law, which for the organic film is:

$$F_{i,o} = \frac{-D_o}{\delta_o} \, \Delta C_{i,o} = \frac{-D_o}{\delta_o} \left(C_{i,o/w} - C_{i,o} \right) \tag{4.5}$$

and analogously in the aqueous film:

$$F_{i,w} = \frac{-D_{aq}}{\delta_w} \, \Delta C_{i,w} = \frac{-D_{aq}}{\delta_w} \left(C_{i,w} - C_{i,w/o} \right) \tag{4.6}$$

where $C_{i,o/w}$, and $C_{i,w/o}$ denote the interfacial concentrations of i in the organic and the aqueous phase, respectively; D_o is the diffusion coefficient in the organic mixture.

Under steady-state conditions, the fluxes in both films are equal. By introducing the partition coefficient of the compound between the organic and aqueous phase ($K_{o/w}$), the total flux can be calculated:

$$K_{o/w} = \frac{C_{i,o/w}}{C_{i,w/o}} \tag{4.7}$$

By combining Eqs. 4.5 to 4.7 the flux is:

$$F_i = F_{i,w} = F_{i,0} = \frac{C_{i,o} - C_{i,w}K_{o/w}}{\frac{\delta_w K_{o/w}}{D_{aq}} + \frac{\delta_o}{D_o}} = \frac{\frac{C_{i,o}}{K_{o/w}} - C_{i,w}}{\frac{\delta_w}{D_{aq}} + \frac{\delta_o}{D_o K_{o/w}}} \tag{4.8}$$

If both films have similar thickness, then the flux will is controlled by $K_{o/w}/D_{aq}$ and $1/D_o$. Since for hydrophobic organic compounds $K_{o/w}$ is much larger than 1, the flux will be controlled by the water film. Thus, the contaminant flux can be approximated using:

$$F_i = \frac{\frac{C_{i,o}}{K_{o/w}} - C_{i,w}}{\frac{\delta_w}{D_{aq}}} \tag{4.9}$$

If the concentrations in the mobile phase are zero (or close to it), then Eq. 1.9 can be further simplified to:

$$F_i = \frac{D_{aq}}{\delta_w} \frac{C_{i,o}}{K_{o/w}} \tag{4.10}$$

where the ratio D_{aq}/δ_w represents the mass transfer coefficient (k [m s^{-1}]); $C_{i,o}/K_{o/w}$ denotes the equilibrium concentration of a compound in water (e.g. its water solubility) and according to Eq. 4.10, the total flux depends linearly on this aqueous concentration at the interface. A change in flow velocity or temperature will affect δ and D_{aq} equally for all compounds involved, resulting in a simultaneous change in the dissolution rate. If the interfacial concentration is increased by adding a surfactant for solubilization, contaminants with low water solubilities are affected the most, as described in the next section.

Fig. 4.2 shows experimental results of the dissolution of PAHs from a coal tar "pool." With increasing flow velocities, fluxes of all PAHs increase simultaneously, indicating that the water film thickness (δ_w) decreases as flow rates increase. Fig. 4.3 illustrates that the observed dissolution rates for a given flow velocity in this experiment are linearly proportional to the respective equilibrium aqueous phase concentrations of the individual PAHs (= $C_{i,o}/K_{o/w}$) as predicted from the film diffusion model. Since D_{aq}, $C_{i,o,}$ and $K_{o/w}$ are known from such type of experiments, the film thicknesses (δ_w) can be calculated. This approach is also valid for solid organic phases such as polymers (e.g., microplastics, passive samplers).
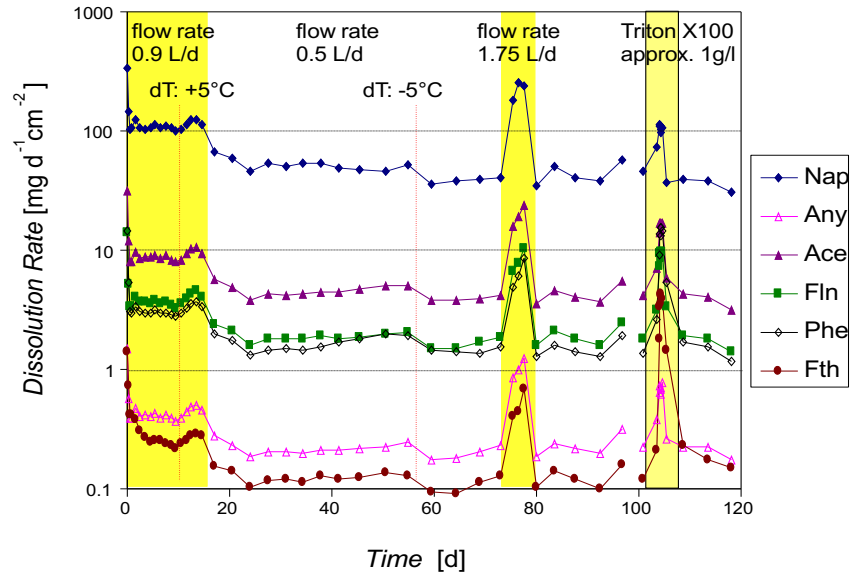
Fig. 4.2: Influence of flow rate (velocity), temperature and surfactants on the dissolution rate of PAHs from a DNAPL (creosote) pool; changes in flow velocity and temperature affect all compound the same way whereas addition of surfactants increases dissolution rates of low solubility compounds most (because of high partitioning into micelles) (Eberhardt, 1995).
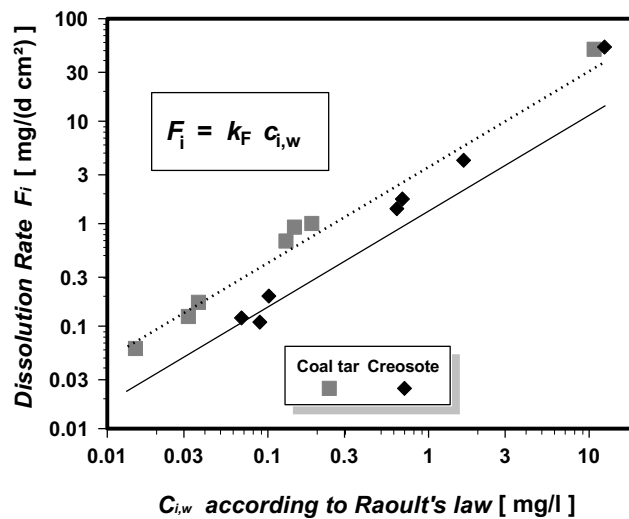
Fig. 4.3: Dissolution rates of PAHs from coal tar and creosote for a given flow velocity are linearly proportional to the respective equilibrium concentration.

5.   REMEDIATION: SOLUBILIZATION BY SURFACTANTS
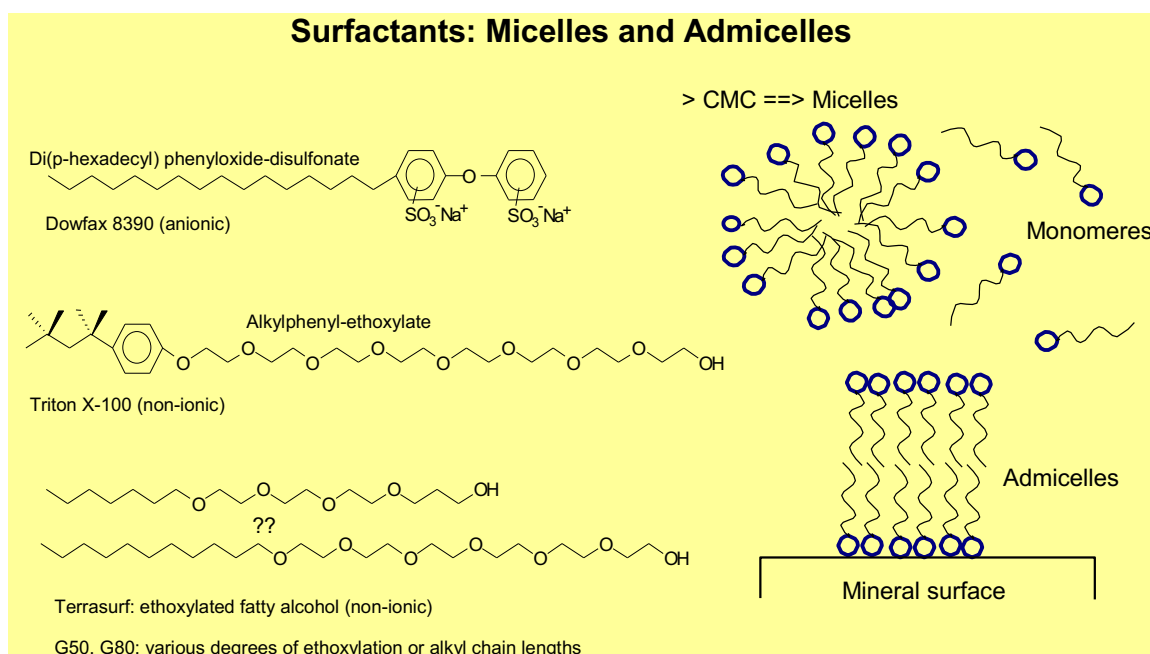
5.1   ENHANCED SOLUBILITY: MICELLES

The dissolution of NAPL can be accelerated if the aqueous concentration at the interface and bulk water are increased by the application of surfactants. Surfactants form aggregates in water - so-called micelles - which can "carry" hydrophobic organic compounds in their interior (see Fig. 5.1). On solid surfaces, they form bilayers (like a membrane) called admicelles. For organic mixtures, surfactants decrease the partition coefficient, which in turn increases the aqueous concentration at the interface. This process is called solubilization. In contrast, mobilization refers to the movement of the NAPL as a separate phase. Micelles form above a certain concentration of surfactants in water, which is known as the critical micelle concentration (CMC - often between 0.1 and 1 g l^{-1}). The relative increase in aqueous solubility (denoted here as S^*) is dependent on the concentration of the surfactant monomers $(C_{mono}$ [kg L^{-1}]), the concentration of micelles $(C_{mic}$ [kg L^{-1}]), and the respective partitioning coefficients K_{mono} and K_{mic} [L kg^{-1}]:

$$S^* = \frac{C_{i,w}}{S_i} = \frac{C_{i,w}}{C_{i,w}^{sat}} = 1 + C_{mono}\, K_{mono} + C_{mic}\, K_{mic}$$

$$\Longrightarrow \ \text{ for } C_{mic} \gg CMC:$$

$$S^* = 1 + C_{mic}\, K_{mic}$$

(5.1)

Fig. 5.2 shows how "solubilization" affects low solubility compounds (= compounds with high K_{OW} values) most. Thus, surfactants "level out" the "solubility" of organic compounds, as shown in Fig. 5.3. Consequently, solubilization leads to faster dissolution, as shown in Fig. 5.4. Solubilization by surfactant micelles is equivalent to adding humic substances or colloidal matter to water, which also take up organic compounds in their hydrophobic moieties.

Fig. 5.1: Examples of common surfactants and steps of structure formation for micelles and admicelles.
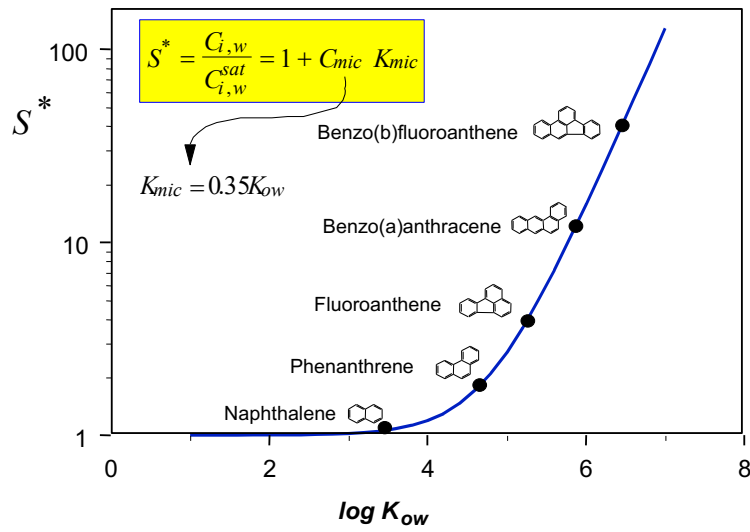
Fig. 5.2: Examples for relative "solubility" enhancement for different organic compounds **(S*: solubility enhancement factor $\cong$ 1 + C_{mic} K_{mic})**
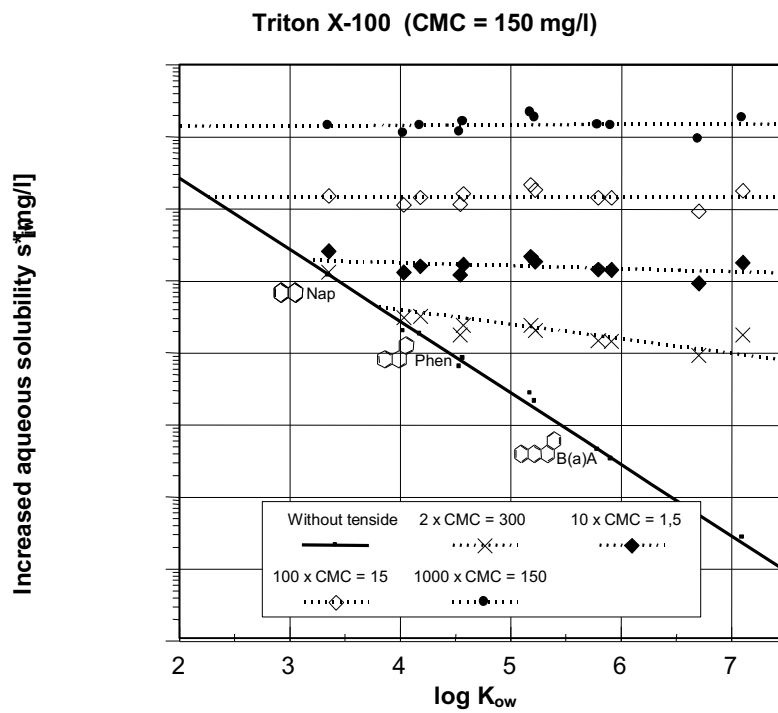
Fig. 5.3: Apparent increases in the solubility in water of the pure substance $s^{*}_{i,w}$ in mg l^{-1} for chosen PAHs in relation to the surfactant concentration above CMC (Triton X-100: commercial surfactant)

Release rates without surfactants

Coal tar in the residual phase (15 cm² per ml)

Release rates with Triton X-100 (2 g/l ca. 10*CMC)
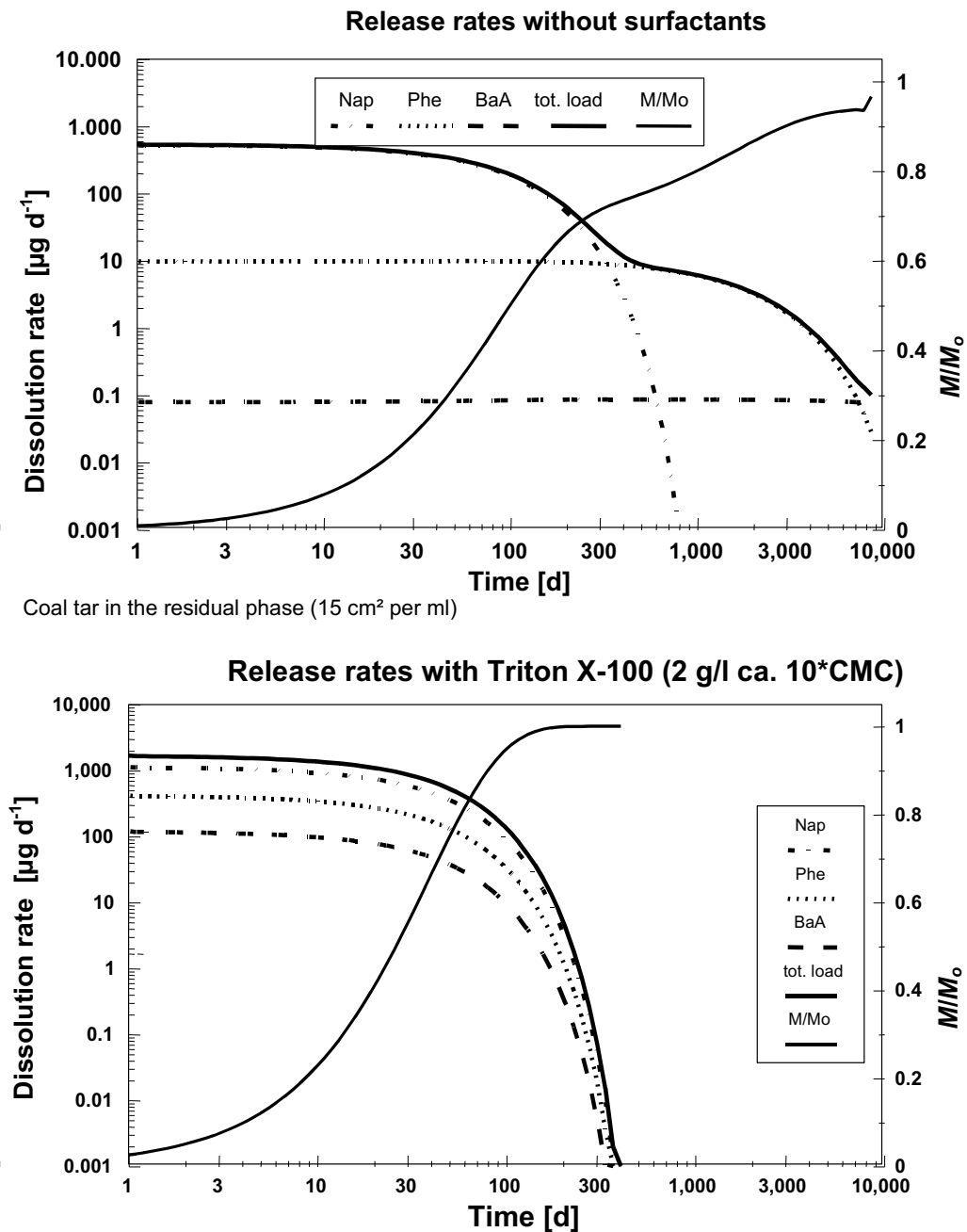
Fig. 5.4: Release rates of Nap, Phe, and BaA from coal tar in residual phase with and without surfactants (calculated after Loyek and Grathwohl, 1996): With the application of surfactants, all PAHs are more or less simultaneously dissolved.

5.2   SORPTION OF SURFACTANTS AND FACILITATED TRANSPORT BY MICELLES

When surfactants are introduced in the subsurface environment, they will as other compounds interact with the solid phase (e.g., minerals). Depending on their surface charge, surfactants adsorb on solid surfaces until the critical micelle concentration is reached (Fig. 5.5). Then a maximum loading of the surface (q_{max} or $C_{s,max}$) with the surfactant is reached and a bilayer may form

27

(admicelles). This sorption behavior is typically described by Langmuir isotherms. Since the surface area is inversely related to grain size, adsorption increases with increasing surface to volume ratio (for spheres = 3/radius) as shown in Fig. 5.5. If sorption is known, the amount of surfactant lost during subsurface remediation can be calculated.
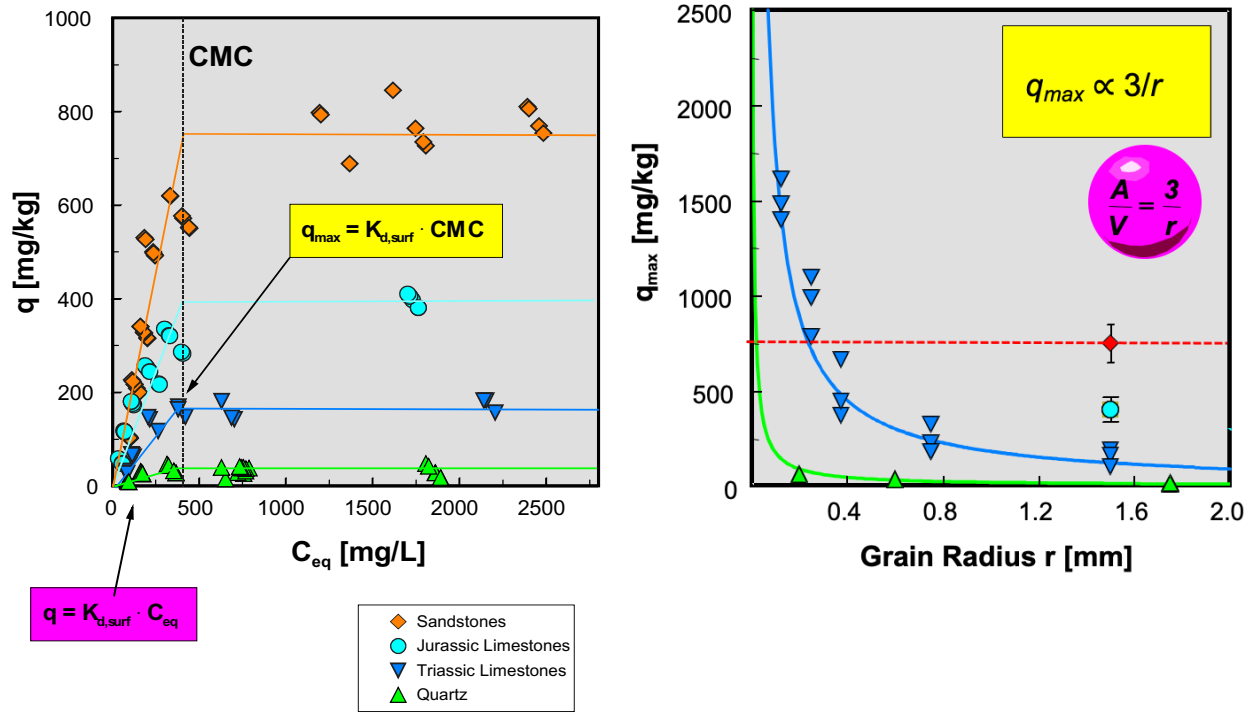
Fig. 5.5: Adsorption of surfactants to different aquifer materials (Terrasurf G50, grain size 2 – 4 mm) and decreasing maximum loading (q_{max}) as a function of the surface to volume ratio (from Danzer and Grathwohl, 1998); sandstones show high adsorption of surfactants because of the internal surface area is accessible to surfactants.

Surfactants adsorbed on solid surfaces form organic coatings (admicelles) which take up organic compounds from water and this causes their retardation during transport. Above the CMC mobile micelles appear in the mobile phase (water) which in turn facilitate transport of organic compounds. Such systems may be used in two ways: Below the CMC, surfactants from "sorptive" barriers and above they facilitate removal of organic pollutants. This was also proposed for humic substances since they behave similarly to surfactants. This behavior is very simply described by the retardation factor:

$$R_d = \frac{total\ concentration}{mobile\ concentration}$$

$$= \frac{C_w\, n + K_{mic}\, C_{mic}\, C_w\, n + K_{oc}\, f_{oc}\, C_w\, \rho_b + K_{adm}\, f_{adm}\, C_w\, \rho_b}{C_w\, n + K_{mic}\, C_{mic}\, C_w\, n}$$

$$= 1 + \frac{K_{oc}\, f_{oc}\, \rho_b + K_{adm}\, f_{adm}\, \rho_b}{n + K_{mic}\, C_{mic}\, n} = 1 + \frac{K_{oc}\, f_{oc} + K_{adm}\, f_{adm}}{1 + K_{mic}\, C_{mic}}\, \frac{\rho_b}{n}$$

$$\text{for } C_{mic} = 0 \tag{5.2}$$

$$R_d = 1 + (K_{oc}\, f_{oc} + K_{adm}\, f_{adm})\, \frac{\rho_b}{n}\ \ \text{(increases with } f_{adm})$$

$$\text{for } K_{mic}\, C_{mic} \gg 1 \ \text{ and } \ K_{adm}\, f_{adm} \gg K_{oc}\, f_{oc}$$

$$\Rightarrow R_d = 1 + \frac{K_{adm}\, f_{adm}}{K_{mic}\, C_{mic}}\frac{\rho_b}{n} \approx 1 + 2\, \frac{f_{adm}}{C_{mic}}\frac{\rho_b}{n}\ \ \text{(decreases with } C_{mic})$$

f_{adm} denotes the fraction of surfactant on the surface analogous to f_{oc} (fraction of organic carbon). C_{mic} is the micelle concentration in water (e.g., kg l^{-1}) and K_{adm} denotes the partition coefficient of the solute between water and admicelles. $K_{oc}\, f_{oc}$ is the distribution coefficient K_d ($K_{oc}\, f_{oc}\, C_w$ and $K_{adm}\, f_{adm}\, C_w$ represent the sorbed or co-sorbed concentration of the compound). Fig. 5.6 illustrates how "solubilization" affects the transport of contaminants – below the CMC the retardation factor increase and above the CMC it decreases again.
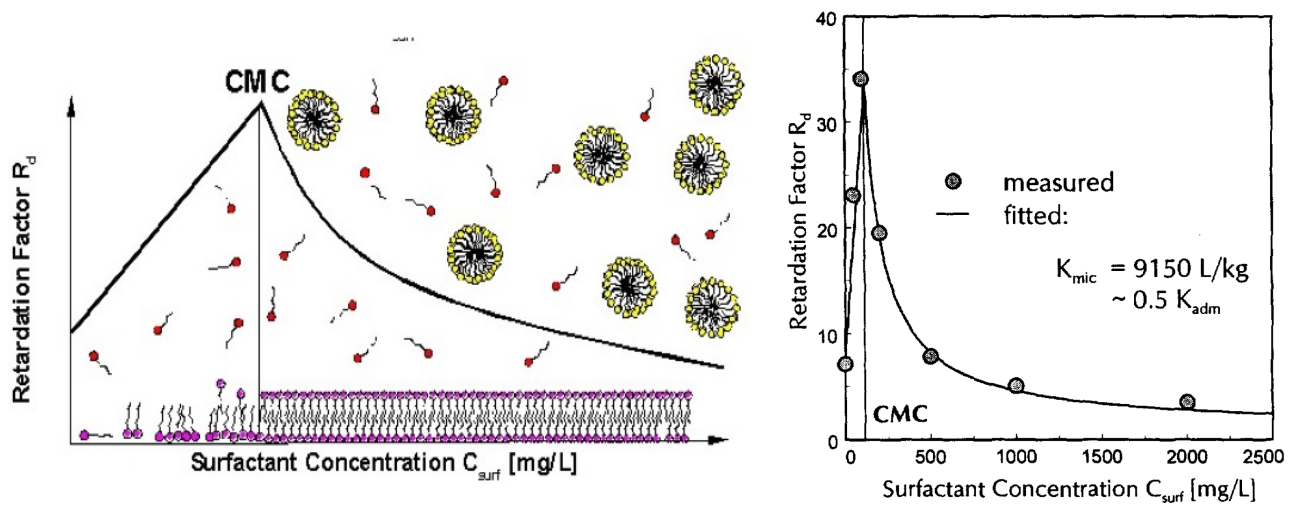
Fig. 5.6: Increase and decrease of the retardation factor for organic compounds with increasing surfactant (Terrasurf G50: ethoxylated fatty alcohol) concentration (from Danzer and Grathwohl, 1998); CMC: Critical Micelle Concentration; measured data from column experiments with phenanthrene in alluvial sand (Neckar): K_d = 1.2 l kg^{-1}, $K_{admicelle}$ = 18300 l kg^{-1}, $K_{d,surf}$ = 2.34 l kg^{-1}.

6.   MORE LITERATURE

Abdul A.S., Gibson T.L. (1991): Laboratory studies of surfactant-enhanced washing of polychlorinated biphenyl from sandy material. Environ. Sci. Technol., 25, 665-671.

Atkins, P.W. (1985): Physical Chemistry. 3rd ed. 857 S. New York (W.H. an and Company)

Banerjee, S. (1984): Solubility of organic mixtures in water. Environ. Sci. Technol. 18, 587-591.

Chiogna, G., Eberhardt, C., Grathwohl, P., Rolle, M. (2010): Evidence of compound dependent hydrodynamic and (hydro)mechanical transverse dispersion with multi-tracer laboratory experiments. Environ. Sci. Technol. DOI: 10.1021/es9023964

Danzer, J., Grathwohl, P. (1998): Coupled transport of PAH and surfactants in natural aquifer materials. Phys. Chem. Earth, Vol. 23, 2, 237-243

Eberhardt, C., Grathwohl, P. (2002): Time scales of pollutants dissolution from complex organic mixtures: blobs and pools. J. Cont. Hydrol., 59, 1-2, 45-66 (Invited paper for Special Issue of J. Cont. Hydrol. on Site Remediation)

Edwards, D.A., Luthy, R.G., Liu, Z. (1991): Solubilization of polycyclic aromatic hydrocarbons in micellar surfactant solutions. Environ. Sci. Technol., 25, 127-133.

Ferreira, S.B., Grathwohl, P., Zuquette, L.V. (2001): Experimental investigations on the dissolution of hydrocarbons from oxygenated gasoline. Journal of Engineering Geology, 27, 3, 208 - 216

Fitzer, E., Fritz, W., Emig.G. (1995): Technische Chemie. Einführung in die chemische Reaktionstechnik. 4. Aufl., 541 S.; Springer, Heidelberg

Fountain, J.C. (1992): Field test of surfactant flooding. Mobility control of dense nonaqueous-phase liquids. In Sabatini & Knox: Transport and Remediation of Subsurface Contaminants. Colloidal, Interfacial, and Surfactant Phenomena. ACS Symposium Series 491.

Fuller, E.N., Schettler, P.D., Giddings, J.C. (1966): A new method for prediction of binary gasphase diffusion coefficients. Ind. Eng. Chem., 58, 19-27

Gauthier, T.H., Seitz, W. R., Grant, C. L. (1987): Effects of structural and compositional variation of dissolved humic materials on Pyren Koc values. Environ. Sci. Technol., 21 (3): 243-248.

Geller, J.T., Hunt, J.R. (1993): Mass transfer from nonaqueous phase liquids in water-saturated porous media. Water Resour. Res. 29(4): 833-845.

Grathwohl, P. (1998): Slow contaminant release: The necessity for enhanced/natural attenuation.- In Kovar, K. and Herbert, M.: Groundwater Quality and Protection, GQ '98 (Proceedings of the Tübingen Conference, Sept. 1998, Invited Paper), IAHS Publ. no. 250, 265 - 272

Grathwohl, P., Reinhard, M. (1993): Desorption of trichloroethylene in aquifer material: Rate limitation at the grain scale. Environ. Sci. Technol., 27 (12): 2360-2366

Hayduk, W., Laudie, H. (1974): Prediction of diffusion coefficients for nonelectrolytes in dilute aqueous solutions. American Institut of Chemical Engineers, Journal, 20 (3): 611-615, New York

Hunt, J.R., Sitar, N., Udell, K.S. (1988): Nonaqueous phase liquid transport and cleanup. 1. Analysis of mechanisms. Water Resour. Res., 24(8), 1247-1258

Imhoff, P.T., Jaffe, P.R., Pinder, G.F. (1993): An experimental study of complete dissolution of a nonaqueous phase liquid in saturated porous media. Water Resour. Res. 30(2): 307-320

Imhoff, P.T., Miller, C.T. (1996): Dissolution fingering during the solubilization of nonaqueous phase liquids in saturated porous media. 1. Modell predictions. Water Resour. Res. 32(7): 1919-1928

Johnson, R. L.; Pankow, J. F. (1992): ''Dissolution of Dense Chlorinated Solvents into Groundwater. 2. Source Functions for Pools of Solvent''. Environ. Sci. Technol., 26, S. 896-901.

Kan, A.T., Tomson, M.B., McRae, T.A. (1992): Chemically enhanced removal of residual aviation gasoline in sandy aquifer material. Comparison of cosolvents and surfactant.- Subsurface Restoration Conference, June 21-24, 1992, Dallas, Texas.

Kile D.E.; Chiou C.T. (1989): Water solubility enhancement of DDT and trichlorbenzene by some surfactants below and above the critical micelle concentration. Environ. Sci. Technol. 23, 832-839.

Klenk, I.D. Grathwohl, P. (2002): Transverse vertical dispersion in groundwater and the capillary fringe. J. Cont. Hydrology, 58, 1-2, 111-128

Lane, W.F., Loehr, R.C. (1992): Estimating the equilibrium aqueous concentration of polynuclear aromatic hydrocarbons in complex mixtures. Environ. Sci. Technol. 26, 983-990.

Lee, L.S., Rao, S.P., Okuda, J. (1992): Equilibrium partitioning of polynuclear aromatic hydrocarbons from coal tar into water. Environ. Sci. Technol. 26, 2110-2115.

Liu, Y., Illangasekare, T.H., Kitanidis, P.K. (2014): Long-term mass transfer and mixing-controlled reactions of a DNAPL plume from persistent residuals. J. Cont. Hydrol., 157, 11–24

Loyek, D., Grathwohl, P. (1996) Ermittlung und Reduzierung der Schadstoffemission bei teer- und teer-ölkontaminierten Böden: Schadstoff-Freisetzung im Kontaminationsherd. PWAB Kolloquium 1996

Lyman, W.L., Reehl, W.F., Rosenblatt, D.H., (eds.) (1990): Handbook of chemical property estimation methods: environmental behavior of organic compounds. (2nd. ed.) New York (Mc Graw - Hill)

Ma, Y.-G., Lei, Y.D. et al. 2010. Critical review and recommended values for the physical-chemical property data of 15 polycyclic aromatic hydrocarbons at 25 °C. J. of Chem. & Eng. Data 55, 819-825.

Mackay, D., Shiu, W.Y. (1977): Aqueous solubility of polynuclear aromatic hydrocarbons. J. of Chem. Engineer. Data 22, 399-402.

Mayer, A. S.; Miller, C. T. (1993): An Experimental Investigation of Pore - Scale Distribution of Nonaqueous Phase Liquids at Residual Saturation. Transport in Porous Media 10, S. 57-80.

Mayer, A.S., Miller, C.T. (1996): The Influence of mass transfer characteristics and porous media heterogeneity on nonaqueous phase dissolution. Water Resour. Res. 32(5): 1551-1567

McCarthy, K.A., Johnson, R.L (1993).: Transport of Volatile Organic Compounds Across the Capillary Fringe. Water Resources Research, 29 (6): 1675-1683

Mersmann, A. (1986): "Stoffübertragung". Springer Verlag.

Miller, C.T., Poirier-McNeill, M.M., Mayer, A.S. (1990): Dissolution of trapped nonaqueous phase liquids: Mass transfer characteristics. Water Resour. Res. 26(11): 2783-2796

Olsson, A.H., Grathwohl, P. (2007): Transverse Dispersion of Non-reactive Tracers in Porous Media: A new Nonlinear Relationship to Predict Dispersion Coefficients. J. Cont. Hydrol., 92, 3-4, 149 - 161

Pankow, J.F., Cherry, J.A. (1996): Dense chlorinated solvents and other DNAPLs in groundwater. Waterloo Press

Powers, S.E., Abriola, L.M., Dunkin, J.S., Weber, W.J.Jr. (1994): Phenomenological models for transient NAPL-water mass-transfer processes. J. Cont. Hydrol. 16: 1-33

Powers, S.E., Loureiro, C.O., Abriola, L.M., Weber, W.J.Jr. (1991): Theoretical study of the significance of nonequilibrium dissolution of nonaqueous phase liquids in subsurface systems. Water Resour. Res. 27(4): 463-477

Ptacek, C.J., Gillham, R.W. (1992): Laboratory and field measurements of non-equilibrium transport in the Borden aquifer, Ontario, Canada. J. Cont. Hydrol., 10: 119-158

Razzaque, M.M., Grathwohl, P. 2008. Predicting organic carbon-water partitioning of hydrophobic organic chemicals in soils and sediments based on water solubility. Water Res. 2008, 42, 3775–3780.

Roberts, P.V., Goltz, M.N., Mackay, D.M. (1986): A natural gradient experiment on solute transport in a sand aquifer: 3. Retardation estimates and mass balances for organic solutes. Water Resour. Res., 22 (13): 2047-2058

Satterfield, C.N. (1970): Mass transfer in heterogeneous catalysis. Cambridge, Ma. (MIT Press), 267 p

Schulz, H.D. (1988): Labormessungen der Sättigungslänge als Maß für die Lösungskinetik von Karbonaten im Grundwasser. Geochimica et Cosmochimica Acta 52: 2651-2657

Schüth, Ch., Grathwohl, P. (1994): Nonequilibrium transport of PAHs: A comparison of column and batch experiments. In: Dracos, T.H., Stauffer, F. (Eds.): Transport and Reactive Processes in Aquifers. Proceedings of the IAHR/AIRH Symposium, April 11-15, 1994, Zürich, Switzerland. (Balkema) Rotterdam, 143-148

Schwille, F. (1984): Leichtflüchtige Chlorkohlenwasserstoffe in porösen und klüftigen Medien. Modell-versuche. Besondere Mitteilungen zum deutschen gewässerkundlichen Jahrbuch, Nr. 46, Koblenz

Travis, C.C., Macinnis, J.M. (1992): Vapor Extraction of organics from subsurface soils: Is it effective? Environ. Sci. Technol., 26, 1885-1887

Travis, C.T., Doty, C.B (1990): Can contaminated aquifers at Superfund sites be remediated? Environ. Sci. Technol., 24, 1464-1466

Valsaraj, K.T.; Thibodeaux, L.J. (1989): Relationship between micelle-water and octanol-water partition constants for hydrophobic organics of environmental interest. Wat. Res. 23, 183-189.

Wayt, H.J., Wilson, D.J. (1989): Soil clean up by in-situ surfactant flushing. II. Theory of micellar solubilization. Separation Science and Technology, 24, (12&13), 905-937.

Werth, C. J., O. A. Cirpka, and P. Grathwohl (2006): Enhanced mixing and reaction through flow focusing in heterogeneous porous media, Water Resour. Res., 42 (12), W12414, doi:10.1029/2005WR004511

Wilke, C.R., Chang, P. (1955): Correlation of diffusion coefficients in dilute solutions. AIChE J., 1: 264-270

Worch, E. (1993): Eine neue Gleichung zur Berechnung von Diffusionskoeffizienten gelöster Stoffe. Vom Wasser, 81: 289-297

Tübingen Dissertations (PhD Theses)

Sayonara Brederode Ferreira (2000): Estudos laboratorias para avaliação potential de contaminação de ãgua e de solo por gasolina oxigenada

Diana Loyek (1998): Die Löslichkeit und Lösungskinetik von polyzyklischen aromatischen Kohlenwasserstoffen (PAK) aus der Teerphase.

Jörg Danzer (1998): Transport of surfactants and coupled transport of polycyclic aromatic hydrocarbons (PAHs) and surfactants in natural aquifer material - laboratory experiments. (https://publikationen.uni-tuebingen.de/xmlui/bitstream/handle/10900/-48821/pdf/49.pdf?sequence=1&isAllowed=y)

Pyka, W. (1994): Freisetzung von Teerinhaltsstoffen aus residualer Teerphase: Laborversuche zur Lösungsrate und Lösungsvermittlung. Tübinger Geowissenschaftliche Arbeiten, Reihe C, 17

APPENDIX

Physicochemical Properties of Gasoline Hydrocarbons

	Hydrocarbon	Density	Molecular Weight	Boiling Point	Water solubility	Vapor Pressure	Henry Constant	Molar Volume	D_g x10^{-2}	D_e x10^{-2}
					25 °C	25 °C	25 °C			
			[g mol^{-1}]	[°C]	[mg l^{-1}]	[kPa]	[-]	[cm^3 mol^{-1}]	[cm^2 s^{-1}]	[cm^2 s^{-1}]
Alcanes	Propane	0.493[1]	44.09	-42.1[1]	62.4[1]					
	i-Butane / n-Butane	0.573[1]	58.14	-0.50[1]	61.4[1]	240.65	38.69	101.47	8.66	0.730
	i-Pentane / n-Pentane	0.626[1]	72.15[1]	36.07	38.5[1]	68.22	50.46	115.22	7.94	0.669
	i-Hexane / n-Hexane	0.660	86.17	69.00	9.5[1]	19.78	68.58[2]	130.51	7.35	0.619
	i-Heptane / n-Heptane	0.684[1]	100.20[1]	98.42	2.93[1]	6.12	92.79[2]	146.56	6.86	0.578
	i-Octane / n-Octane	0.703	114.23[1]	126.00	0.66[1]	1.94	121.00[2]	162.49	6.46	0.544
	Nonane	0.718[1]	128.25	150.80	0.22[1,2]	0.67	138.00	178.70	6.13	0.516
	Decane	0.730[1]	142.28[1]	174.10	0.052[1,2]	0.24	197.85[3]	203.12	5.71	0.481
Alcenes	Butene	0.588[1]	56.11[1]	-6.2[1]	222[1]	289.17	10.21	95.41	8.95	0.753
	Pentene	0.626	70.13[1]	30.0	148[1]	84.87	16.34	112.03	8.07	0.680
	Hexene	0.670	84.17	63.4[1]	50[1]	24.56	12.38	125.03	7.51	0.632
	Heptene	0.697	98.19[1]	93.4	14.1	7.50	16.34	140.88	7.00	0.589
	Octene	0.715	112.22[1]	121.3	2.7[1]	2.36	25.53	156.97	6.58	0.554
	Nonene	0.729	126.24[1]	146.88[1]	0.63	0.79	34.04	173.12	6.22	0.524
	Decene	0.741	140.19	170.5	0.1	0.28	34.50	189.24	5.92	0.499
Aromatics	Benzene	0.874	78.11	80.1[6]	1780	9.08	0.22[4]	89.37	8.74	0.736
	Toluene	0.865	92.14	110.6	534.8	3.70	0.24[4]	106.52	7.95	0.670
	o-. m-. p-Xylene	0.868	106.17	140.2	166	1.06	0.26[5]	122.26	7.38	0.621
	Ethylbenzene	0.867	106.20	136.2[6]	161.2	1.25	0.25	122.49	7.37	0.621
	Trimethylbenzene	0.873	120.19	164.48	57	0.36	0.28	137.67	6.92	0.583
	Ethanol	0.780	46.10	78.5[6]	c.m.	7.90[6]	3.4E-04[3]			
	Methanol		32.00		c.m.					
	MTBE	0.776	88.15	55.0	48000	33.84	0.03	113.60	0.07778	0.00655

Water solubility: Brookman, G.T., Flanagan, M., Kebe, J.O. (1995). Literature Survey: Hydrocarbon Solubility and Attenuation Mechanisms. Am. Petroleum Inst., Washington, DC, Pub. No. 441. Mean Solubility o-Xylene (175 mg/l) and p-Xylene (157 mg/l). Mean Solubility from 1,2,3-Trimethylbenzene (65.3 mg/l), 1,2,4-Trimethylbenzene (57 mg/l) and 1,3,5-Trimethylbenzene (48.2 mg/l). RIPPEN Handbuch der Umweltchemikalien. Stoffdaten, Prüfverfahren, Vorschriften. - Loseblattsammlung, 7 Bd., 41.

Ergänzungslieferung 1997. [1] Verbruggen et al. (2000); [2] Mackay et al. (1993); [3] Yaws and Yang (1992); [4] Peng and Wan (1997); [5] EPA (2000); [6] Reisinger and Grathwohl (1996).

Saturation Concentrations of Hydrocarbons for Gasoline Mixtures: ARAL (2002)[1] and PETROBRAS (1997)

	Hydrocarbon	Gasolina Composition [Weight %]				C_g^{sat} [g m^{-3}] Raoul's Law				C_w^{sat} [g m^{-3}] Raoul's Law			
		Normal **ARAL**	Super **ARAL**	Super Plus **ARAL**	Gasoline A **PETROBRAS**	Normal **ARAL**	Super **ARAL**	Super Plus **ARAL**	Gasoline A **PETROBRAS**	Normal **ARAL**	Super **ARAL**	Super Plus **ARAL**	Gasoline A **PETROBRAS**
Alcanes	Propane	< 0.1	< 0.1	< 0.1	1.0				335.37				1.24
	i-Butane / n-Butane	4.7	5	6.7	14.1	400.98	426.58	571.62	1202.95	4.36	4.64	6.22	13.09
	i-Pentane / n-Pentane	17.8	15.4	10.6	17.5	430.51	372.46	256.37	423.26	8.57	7.41	5.10	8.42
	i-Hexane / n-Hexane	17.3	13.7	9	3.0	121.29	96.05	63.10	21.03	1.67	1.32	0.87	0.29
	i-Heptane / n-Heptane	6.8	4.5	6.6	8.7	14.74	9.76	14.31	18.86	0.17	0.12	0.17	0.22
	i-Octane / n-Octane	7.9	8	16.6	1.2	5.43	5.50	11.41	0.82	0.04	0.04	0.08	0.01
	Nonane	1.3	1.3	0.8	3.1	0.31	0.307	0.189	0.732	0.0011	0.0011	0.0007	0.0026
	Decane	2.5	1.1	1.1	1.0	0.21	0.093	0.093	0.084	0.0003	0.0001	0.0001	0.0001
	Total of Alcanes	**58.3**	**49**	**51.4**	**49.6**								
Alcenes	Butene	2.5	0.3	1.3	0	256.29	30.75	133.27	0.00	8.70	1.04	4.52	0.00
	Pentene	3.3	3	3.8	0.3	99.28	90.26	114.33	9.03	6.12	5.57	7.05	0.56
	Hexene	2.2	2	2.1	0.3	19.15	17.41	18.28	2.61	1.15	1.04	1.10	0.16
	Heptene	0.9	0.8	0.8	2.0	2.39	2.13	2.13	5.32	0.11	0.10	0.10	0.25
	Octene	0.4	0.4	0.3	1.3	0.34	0.34	0.25	1.090	0.0085	0.0085	0.0063	0.0275
	Nonene	1.2	1	0.7	0.2	0.34	0.28	0.20	0.056	0.0053	0.0044	0.0031	0.0009
	Decene	1.2	0.8	0.4	0.2	0.12	0.08	0.04	0.020	0.0008	0.0005	0.0003	0.0001
	Total of Alcenes	**11.7**	**8.3**	**9.4**	**4.3**								
Aromatics	Benzene	0.7	0.8	0.5	1.0	2.25	2.58	1.61	3.22	14.02	16.03	10.02	20.03
	Toluene	6.9	10.9	8.4	3.0	9.06	14.30	11.02	3.94	33.90	53.56	41.27	14.74
	o-. m-. p-Xylene	5.5	6	8.1	5.7	2.06	2.25	3.03	2.13	7.56	8.25	11.13	7.83
	Ethylbenzene	1.4	2.1	2.2		0.62	0.93	0.98	0.00	1.87	2.80	2.94	0.00
	Trimethylbenzene	9.3	12.3	7	5.6	1.20	1.59	0.91	0.72	3.88	5.13	2.92	2.33
	Total of Aromatics	**23.8**	**32.1**	**26.2**	**18.3**								
	Ethanol	0	0	0	21.0				58.81				
	Methanol	0	0	0	2.4								
	MTBE	0-1.1	0-5.4	0-13.5	0.1	13.19	64.77	155.94	1.20	526.56	2584.94	6223.01	47.87
	Σ Hydrocarbons	**94.9**	**94.8**	**100**	**95.7**								

[1] Source of Hydrocarbon Composition from Gasoline: Januar 2002: Aral.de [www.aral.de/corporate/]

Saturation Concentrations of Hydrocarbons from Kerosine

	Hydrocarbon	Density [g mL^{-1}]	Molecular Weight [g mol^{-1}]	Boiling Point °C	Water Solubility S_i^w or $S_{i,scl}^w$ 25 °C [mg l^{-1}]	Vapor Pressure P^o or P_L 25 °C [kPa]	Henry Constant 25 °C [-]	Composition Kerosene Weight%	C_g^{sat} [g m^{-3}]	C_w^{sat} [g m^{-3}]
Alkyl-Mono-aromatics	1,2,3,4-Tetramethylbenzene	0.901[12]	134.22	205.0	33.94	0.048[1]	0.327	1.1	3.69E-02	4.81E-01
Branched Alkanes	Isodecane	0.768	142.28		0.022	0.319[2]	217.00	1.3	2.89E-01	3.48E-04
	Isoundecane							1.2		
	Isododecane							1.2		
	Isotridecane							0.9		
	Isotetradecane							0.6		
Mono-aromatics	Indene	0.997[12]	116.16		332.40	0.147[3]	0.06	0.00026	2.66E-05	1.29E-03
	Tetralin THN	0.970[12]	132.20	207.65	47.00	0.049[3]	0.06	0.27	9.24E-03	1.66E-01
	1-Methyltetralin		146.23					0.65		
	2-Methyltetralin		146.23					0.68		
n-Alkanes	n-Heptane	0.684	100.20	98.42	2.93	6.110[4]	92.79	0.73	3.11E+00	3.69E-02
	n-Octane	0.703	114.23	125.7	0.66	1.804[4]	121.00	1.6	2.01E+00	1.60E-02
	n-Nonane	0.718	128.25	150.8	0.122	0.571[4]	138.00	2.3	9.17E-01	3.79E-03
	n-Decane	0.730	148.28	174.1	2.20E-03	0.175[4]	197.85	3.2	3.91E-01	8.21E-05
	n-Undecane	0.740	156.31	195.9	4.40E-03	0.052[4]	75.70	5.2	1.89E-01	2.53E-04
	n-Dodecane	0.749	170.34	216.3	3.70E-03	0.016[4]	296.77	6.8	7.45E-02	2.56E-04
	n-Tridecane	0.756	185.36		4.70E-03	5.29E-03[5]	95.06	3.3	1.22E-02	1.45E-04
	n-Tetradecane	0.763	198.40	252.0	6.96E-03	3.88E-03[4]	14.00	3.3	8.93E-03	2.00E-04
	n-Pentadecane	0.769	212.42	270.0	7.60E-05	1.55E-03[4]	19.46	2.2	2.38E-03	1.36E-06
	n-Hexadecane	0.773	226.44	287.0	6.28E-03	6.38E-04[4]	1.31	0.7	3.12E-04	3.36E-05
	n-Heptadecane	0.778	240.48	303.0	2.94E-04	2.72E-04[4]	2.27	0.4	7.58E-05	8.45E-07
	n-Octadecane	0.777	254.40	317.0	2.26E-03	1.50E-04[6]	0.37	0.3	3.14E-05	4.61E-06
	n-Nonadecane	0.786	268.53	330.0	3.49E-05	7.77E-05[6]	0.12	0.2	1.08E-05	4.50E-08
	n-Eicosane	0.789	282.60		2.49E-04	6.61E-05[6]	0.0132	0.1	4.61E-06	1.52E-07
	n-Heneicosane		296.58		4.13E-08			0.1		

Saturation Concentrations of Hydrocarbons from Kerosine (cont.)

	Hydrocarbon	Density	Molecular Weight	Boiling Point	Water Solubility S_i^w or $S_{i,scl}^w$	Vapor Pressure P^o or P_L	Henry Constant	Composition Kerosene	C_g^{sat}	C_w^{sat}
		[g mL^{-1}]	[g mol^{-1}]	°C	25 °C [mg l^{-1}]	25 °C [kPa]	25 °C [-]	Weight%	[g m^{-3}]	[g m^{-3}]
Naphthalenes	Naphthalene	1.030	128.19	218	105.67	4.19E-02[7]	0.0179	0.31	9.06E-03	0.4421
	1-Methylnaphthalene	1.022	142.20	244.6	28.05	8.84E-03[9]	0.0106	0.54	3.33E-03	0.1842
	2-Methylnaphthalene	1.006	142.19	241.6	29.53	1.12E-02[8]	0.0207	1.1	8.60E-03	0.3953
	1,4-Dimethylnaphthalene	1.017	156.23	262	11.40	2.27E-03[9]	0.0126	0.19	3.01E-04	0.0240
Diaromatics (Except Naphthalenes)	Fluorene	1.202	166.00	295	12.38	7.92E-04[7]	0.0393	0.0042	2.32E-06	5.42E-04
Polynuclear Aromatics	Acenaphthene	1.190	154.21	277.5	19.65	1.52E-03[8]	6.33E-03	0.0047	4.98E-06	1.04E-03
	Acenaphthylene	0.890	152.20	265-275	44.56	4.14E-03[8]	4.66E-03	0.0045	1.30E-05	2.28E-03
	Anthracene	1.283	178.24	340	5.00	8.65E-05[7]	2.28E-03	0.00012	7.24E-09	5.82E-06
	Phenanthrene	1.030	178.24	339	4.21	1.34E-04[7]	1.46E-03	0.0058	5.42E-07	2.37E-04
	2-Methylanthracene		192.26	359	1.28	6.68E-06[10]	0.0023	0.00046	2.14E-09	5.29E-06
	9,10-Dimethylanthracene		206.29		2.04	3.65E-07[10]	0.0012	0.00071	1.81E-10	1.21E-05
	Fluoranthene	1.252	202.26	375	1.24	8.72E-06[8]	7.91E-04	0.00086	5.23E-09	9.11E-06
	Pyrene	1.271	202.26	360	1.18	1.58E-05[7]	4.88E-04	0.00024	2.65E-09	2.43E-06
	Benzo(b)fluorene		216.28	402	0.27	7.33E-09[11]	1.60E-04	0.00012	6.14E-13	2.58E-07
	Benzo(a)fluorene		216.28	407	1.89	6.24E-07[10]	1.09E-03	0.00009	3.92E-11	1.36E-06
	7,12-Dimethylbenz(a)anthracene		256.35		0.56	2.67E-08[10]	8.30E-05	0.002	3.72E-11	7.57E-06
	Total of known							**40.49**		
	11 EPA-PAK without Nap							**0.0196**		
	Average Value	**0.80**	**173**							

Saturation Concentrations of Hydrocarbons from Diesel Fuel

Hydrocarbon	Density [g mL^{-1}]	Molecular Weight [g mol^{-1}]	Boiling Point °C	Water Solubility S_i^w or $S_{i,scl}^w$ 25 °C [mg l^{-1}]	Vapor Pressure P° or P_L 25 °C [kPa]	Henry Constant 25 °C [-]	Composition Diesel Weight%	C_g^{sat} [g m^{-3}]	C_w^{sat} [g m^{-3}]
Phenanthrene		178.24	339	6.220	1.34E-04	1.46E-03	2.24E-02	2.18E-06	1.41E-03
Antracene		178.24	340	3.271	8.65E-05	2.28E-03	6.67E-04	4.19E-08	2.20E-05
Fluoranthene		202.26	375	1.710	8.72E-06	7.91E-04	4.53E-04	2.86E-09	6.89E-06
Pyrene		202.26	360	2.383	1.58E-05	4.88E-04	3.42E-02	3.92E-07	7.25E-04
Benz(a)antracene		228.3	437.6	0.036	5.43E-07	4.91E-04	5.96E-05	2.35E-11	1.69E-08
Chrysene		228.3	448.0	0.403	1.07E-07	2.14E-04	4.29E-04	3.33E-11	1.36E-06
Benzo(b)fluoranthene		252.32	480.0	0.039	1.30E-09	2.69E-05	2.38E-05	2.25E-14	6.59E-09
Benzo(k)fluoranthene		252.32	480.0	0.063	4.12E-09	2.39E-05	1.19E-05	3.56E-14	5.36E-09
Benzo(a)pyrene		252.32	495.0	0.051	7.28E-09	1.87E-05	1.19E-05	6.29E-14	4.32E-09
Benzo(ghi)perylene		276.34	525.0	0.082	2.25E-08	1.35E-05	1.19E-05	1.95E-13	6.37E-09
3-Methylphenanthrene		192.26	350.0	0.653	6.68E-06		2.50E-02	1.21E-07	
2-Methylphenanthrene		192.26	155-160	0.593	6.68E-06		2.14E-02	1.04E-07	
2-Methylanthracene		192.26	359.0	1.400	6.68E-06		3.33E-04	1.62E-09	4.37E-06
4H-cyclopenta(def)phenanthrene		190.25	353.0	8.331	4.16E-06		3.57E-04	1.08E-09	
9-Methylphenanthrene		192.26		0.152			1.03E-02		
1-Methylphenanthrene		192.26	359.0	0.152	6.68E-06		9.28E-03	4.50E-08	
2-phenylnaphthalene		204.27	345.5				2.23E-03		
3,6-Dimethylphenanthrene		206.29		1.094	2.43E-06		8.84E-03	1.56E-08	
3,9-Dimethylphenanthrene		206.29					2.45E-02		
Benzo(a)fluorene		216.28	407	0.026	6.24E-07	1.09E-03	1.19E-05	5.39E-12	2.55E-09
Retene		234.34	390-394				2.62E-04		
Benzo(b)fluorene			402	0.2690	7.33E-09	1.60E-04	1.19E-05	6.34E-14	2.67E-08
2-Methylpyrene				0.331			2.56E-02		
4-Methylpyrene							7.50E-04		
1-Methylpyrene			410	0.331	2.33E-07		5.96E-02	1.01E-08	
3-Methylchrysene							3.93E-04		
2-Methylchrysene							1.91E-04		
1-Methylchrysene							5.72E-04		
Benzo(e)pyrene			311	0.202	2.53E-08		3.57E-05	6.56E-13	
Coronene	C24H12	525	300.36	1.658	1.774E-11		1.19E-05	1.53E-16	1.77E-07
Dibenzothiophene	C12H8S	332.5	184.26	7.562	2.73E-05		3.57E-05	7.09E-10	

Source of the composition data: Comparison of Exhaust Emissions from Swedish Environmental Classified Diesel Fuel (MK1) and European Program on Emissions, Fuels and Engine Technologies (EPEFE) Reference Fuel: A Chemical and Biological Characterization, with Viewpoints on Cancer Risk. R. Westerholm, A. Christensen, M.Törnqvist, L. Ehrenberg, U. Rannung, M. Syörgen, J. Rafter, C. Soontjens, J. Almén, K. Grägg, Environ. Sci. Technol. 2001, 35, 1748-1754.

$S_{i,scl}^w$ and P_L are the subcooled solubility and liquid-vapor pressure in grey color, respectively.